Scale effects on the elastic behavior of periodic and hierarchical two-dimensional composites

S. Pecullan, L.V. Gibiansky, S. Torquato*

*Department of Civil Engineering and Operations Research and Princeton Materials Institute,
Princeton University, Princeton, NJ 08544, U.S.A.*

Abstract

The apparent stiffness tensors of two-dimensional elastic composite samples smaller than the representative volume element (RVE) are studied as a function of system size. Numerical experiments are used to investigate how the apparent properties of the composite converge with increasing scale factor n, defined to be the ratio between the linear size of the composite and the linear size of the unit cell. Under affine (Dirichlet-type) or homogeneous stress (Neumann-type) boundary conditions, the apparent elastic moduli overestimate or underestimate, respectively, the effective elastic moduli of the infinitely periodic system. The results show that the difference between the Dirichlet, Neumann and the effective stiffness tensors depends strongly on the phase stiffness contrast ratio. Dirichlet boundary conditions provide a more accurate estimate of the effective elastic properties of stiff matrix composites, whereas Neumann boundary conditions provide a more accurate estimate for compliant matrix structures. It is shown that the apparent bulk and shear moduli may lie outside of the Hashin–Shtrikman bounds. However, these bounds provide good upper and lower estimates for the apparent bulk and shear moduli of structures with a scale factor $n \geqslant 2$. A similar approach is used to study hierarchical composites containing two distinct structural levels with a finite separation of length scales. It is shown, numerically, that the error associated with replacing the smallest-scale regions by an equivalent homogeneous medium is very small, even when the ratio between the length scales is as low as three. © 1999 Elsevier Science Ltd. All rights reserved.

Keywords: A. Microstructures; Scale effects; B. Elastic material; Particulate reinforced material; C. Finite elements

1. Introduction

It is known that under a sufficiently smooth external field, a composite behaves as an equivalent homogeneous material (see, e.g., Christensen, 1979). For infinitely

---

* Corresponding author. E-mail: torquato@matter.princeton.edu

periodic composite media, the calculation of their effective properties reduces to obtaining relevant fields (such as electric and strain fields) in a unit cell subject to periodic boundary conditions. However, such a description is correct only asymptotically, when the characteristic wavelength of the field is large compared with the size of the periodic cell and may not be valid near the boundary of the composite sample where the fields are clearly not periodic.

This last restriction is of great relevance for practical applications. Indeed, now one can fabricate composite structures consisting of a finite number of cubic cells (see, e.g., Sigmund et al., 1998). However, standard methods of measurement are designed for homogeneous materials subject to homogeneous boundary conditions. They may produce apparent properties that are far from the effective properties of the composites. Therefore, natural and important questions to ask are the following: how large does the scale factor n (that we define as the ratio between the linear size of the composite sample and the linear size of the periodic cell) have to be to produce apparent properties that are close to the theoretical values? How does the error in the measurement of the apparent overall properties using homogeneous boundary conditions depend on the scale factor of the sample? The study of these questions is the first goal of the present work.

Clearly, for a sufficiently large scale factor and finite ratio of the phase properties, the apparent properties will approach the effective properties of the infinitely periodic medium. This condition may provide a rough measure of the 'representative volume element' (RVE). We will estimate (for the examples considered) the size of the RVE. Note that our measure differs from the common definition of the RVE. For random composites, it is usually defined by considering variations of the fields averaged over some window placed at some random position inside the medium. For ergodic composites with homogeneous (on infinity) boundary conditions and a sufficiently large window size, these variations vanish. Thus, the size of the window that allows the 'smoothing out' of all variations is called a representative volume element. Note that strain and stress fields in a random composite are not affected by such a 'passive' window because it does not influence the solution of the elasticity problem, but only delineates the region for averaging. On the contrary, in our study we will impose homogeneous (strain or stress) conditions on the boundary of the window, thus inducing the fields inside the window. As we will see, this results in a much more conservative estimate of the RVE size. We believe that our measure is appropriate for studying effects of the boundary conditions on the fields inside the composite. This is especially important if the ratio of the size of the periodic cell to the size of the sample is not very small.

Composite structures may often be employed as elements of larger structures in which the difference in scale between material phases is necessarily some finite value. For example, in the design of piezocomposites (Sigmund et al., 1998), the composite matrix (composed of a finite number of cells) is fiber reinforced by aligned piezoceramic rods whose diameters are comparable to the size of the unit cell of the matrix. This poses the question of whether theoretical descriptions based on an infinite separation of length scales adequately describes the experimental conditions. Therefore, the second goal of the present work is to investigate scale effects on the

behavior of hierarchical (i.e., multi-scale) composites with large but finite separation of scales. In particular, we seek to determine the error in calculating the effective properties of two-scale composites when we replace the smallest-scale regions by equivalent homogeneous media. Additionally, we also study the effects of the scale factor on the apparent properties of the two-scale composite.

The main tool of our analyses is numerical experiment via the method of finite elements. To save computational time, we will consider the two-dimensional version of the posed problem. As we will see, the results are sufficiently convincing to ensure generalization to the three-dimensional problem. These results also have independent theoretical significance.

Specifically, consider a unit square made of an $n \times n$ set of elementary cells of composite materials with the scale factor n changing from 1 to 6 in our experiments. We impose homogeneous displacement or traction conditions on the boundary, solve the linear elasticity problem numerically and compute average strain and average stress tensors. The average strain tensor is proportional to the average stress tensor in these experiments, which allows us to introduce stiffness tensors relating average fields when affine displacement (Dirichlet-type) and homogeneous traction (Neumann-type) boundary conditions are specified. Huet (1990) named these same tensors kinematic apparent modulus and static apparent modulus tensors, respectively. We will refer to these as Dirichlet and Neumann stiffness tensors, which are not equal, in general. However, one can show that the converge and equal the standard effective stiffness tensor in the limit $n = \infty$. We study (both theoretically and numerically) the relations between the Dirichlet and Neumann stiffness tensors for variable scale factor n.

We concentrate on several model problems for two-dimensional linear elastic composites. For three elementary cells with different microstructures, we study how rapidly the coefficients of the Dirichlet and Neumann stiffness tensor converge (with increasing n) to the corresponding values for the effective stiffness tensor. Subsequently, we study more complex unit squares possessing two length scales. We will be interested in knowing whether one can reduce the two-scale problem to a one-scale problem by using the concept of the effective properties. Our goal is to develop specific recommendations on how to compute effective properties of such composites.

The present study is closely related to the one conducted by Huet (1990) who introduced the concept of apparent properties for the Dirichlet-type and Neumann-type boundary conditions. Hazanov and Huet (1994) and Hazanov and Amieur (1995) generalized this concept to mixed boundary conditions. Similar problems were also considered by Ostoja-Starzewski (1993, 1996, 1998) who numerically investigated statistical characteristics of the Dirichlet and Neumann tensor for the anti-plane shear problem. There are, however, important differences between these studies and the present work. We study periodic composites with predetermined structure and a sample (represented by the unit square in this paper) that always includes an integral number of elementary cells. Thus, the phase volume fractions in each sample under study are equal to the average phase volume fractions. A natural question arises as to whether one can propose tighter bounds on the Dirichlet and Neumann stiffness tensors than the corresponding arithmetic–harmonic mean bounds obtained by Huet

(1990). In some of our examples the elastic tensor is square symmetric or even isotropic. We will compare the Dirichlet and Neumann bulk and shear moduli of these nearly isotropic structures with the corresponding Hashin–Shtrikman (1963) bounds and show that they may not satisfy these bounds.

Another relevant problem was studied by Drugan and Willis (1996). They derived the non-local correction to the effective property tensor that depends on the derivative of the average strain field over the slow coordinate. Based on this analysis, they derived estimates on the minimum RVE size, i.e., the size of the element for which the effective stiffness tensor adequately describes the composite. We will compare their conclusions with our results.

The structure of the paper is the following: in Section 2 we define several tensors that characterize an apparent stiffness of the composite sample and describe the numerical method that was used to compute these tensors. In Section 3, we consider the so-called one-scale composite with structural elements of similar characteristic size. We compute Dirichlet, Neumann and the effective stiffness of these microstructures for different scale factors. In Section 4 we consider hierarchical composites with two distinct length scales. In Section 5 we summarize our findings.

2. Apparent stiffness of the unit cell

Consider a unit square of a two-phase composite material. The system is described by the linear elasticity equations

$$\boldsymbol{\sigma}(\boldsymbol{x}) = \boldsymbol{C}(\boldsymbol{x}) : \boldsymbol{\varepsilon}(\boldsymbol{x}), \quad \nabla \cdot \boldsymbol{\sigma}(\boldsymbol{x}) = 0, \quad \boldsymbol{\varepsilon}(\boldsymbol{x}) = \tfrac{1}{2}[\nabla \boldsymbol{u}(\boldsymbol{x}) + (\nabla \boldsymbol{u}(\boldsymbol{x}))^{\mathrm{T}}], \tag{1}$$

where $\boldsymbol{u}$ is the displacement vector, $\boldsymbol{\sigma}$ and $\boldsymbol{\varepsilon}$ are the stress and the strain tensors, respectively, the symbol : denotes contraction over two indices, and $\boldsymbol{C}$ is the stiffness tensor of the material. For a two-phase composite the stiffness tensor $\boldsymbol{C}(\boldsymbol{x})$ depends on the vector $\boldsymbol{x}$ as follows

$$\boldsymbol{C}(\boldsymbol{x}) = \chi_1(\boldsymbol{x})\boldsymbol{C}_1 + \chi_2(\boldsymbol{x})\boldsymbol{C}_2, \tag{2}$$

where $\boldsymbol{C}_1$ and $\boldsymbol{C}_2$ are the phase stiffness tensors and $\chi_i(\boldsymbol{x})$ are the characteristic functions of the regions occupied by the phase i, $i = 1, 2$. For isotropic phases, the stiffness tensors are defined by the bulk moduli κ_i and the shear moduli μ_i. In two dimensions, these moduli depend on the Young's modulus E_i and the Poisson's ratios v_i as

$$\kappa_i = \frac{E_i}{2(1 - v_i)}, \quad \mu_i = \frac{E_i}{2(1 + v_i)}. \tag{3}$$

The most common measure of the overall stiffness of periodic or random composites is the effective stiffness tensor given by homogenization theory (Christensen, 1979; Sanchez-Palencia, 1980). However, in some situations two other measures may be helpful. We will discuss all three here together with the numerical procedure that we will use to calculate them.

2.1. Effective stiffness tensor

Consider the problem (1) with three different periodic boundary conditions

$$\varepsilon^{(i)}(x) \text{ is periodic}, \quad \langle \varepsilon(x) \rangle = a^{(i)}, \quad i = 1, 2, 3, \tag{4}$$

where the angular brackets denote averaging over the unit square and

$$a^{(1)} = \frac{1}{\sqrt{2}} \begin{pmatrix} 1 & 0 \\ 0 & 1 \end{pmatrix}, \quad a^{(2)} = \frac{1}{\sqrt{2}} \begin{pmatrix} 1 & 0 \\ 0 & -1 \end{pmatrix}, \quad a^{(3)} = \frac{1}{\sqrt{2}} \begin{pmatrix} 0 & 1 \\ 1 & 0 \end{pmatrix} \tag{5}$$

are three linearly independent second-order tensors. Note that they form a basis for second-order symmetric tensors in two dimensions. Moreover, an isotropic stiffness tensor with the bulk modulus κ and shear modulus μ can be represented as

$$C = 2\kappa a^{(1)} a^{(1)} + 2\mu (a^{(2)} a^{(2)} + a^{(3)} a^{(3)}) \tag{6}$$

in such a basis.

One can solve each of the problems (1) and (4) numerically, find the local strain and stress tensors $\varepsilon^{(i)}(x)$ and $\sigma^{(i)}(x)$ and calculate the average strain and stress tensors

$$\bar{\varepsilon}^{(i)} = \langle \varepsilon^{(i)}(x) \rangle, \quad \bar{\sigma}^{(i)} = \langle \sigma^{(i)}(x) \rangle. \tag{7}$$

The linearity of the problem allows us to introduce an effective stiffness tensor C_* of the cell via the set of equations

$$\bar{\sigma}^{(i)} = C_* : \bar{\varepsilon}^{(i)}, \quad i = 1, 2, 3. \tag{8}$$

This is the most common definition of the overall properties of a composite material. The effective stiffness tensor can be equivalently defined by the minimum energy variational principle

$$a^{(i)} : C_* : a^{(i)} = \min_{\substack{\text{periodic } \varepsilon(x) \\ \varepsilon(x) = \frac{1}{2}[\nabla u(x) + (\nabla u(x))^{\mathrm{T}}] \\ \langle \varepsilon(x) \rangle = a^{(i)}}} \langle \varepsilon(x) : C(x) : \varepsilon(x) \rangle, \quad i = 1, 2, 3. \tag{9}$$

Alternatively, the effective compliance tensor can be defined via the equations

$$\bar{\varepsilon}^{(i)} = S_* : \bar{\sigma}^{(i)}, \quad i = 1, 2, 3, \tag{10}$$

where $\bar{\varepsilon}^{(i)}$ and $\bar{\sigma}^{(i)}$ are the average strain and stress fields for the solution of the problem (1) with periodic stress boundary conditions

$$\sigma^{(i)}(x) \text{ is periodic}, \quad \langle \sigma(x) \rangle = a^{(i)}, \quad i = 1, 2, 3. \tag{11}$$

Equivalently, it can be defined by the minimum complementary energy principle in the form

$$a^{(i)} : S_* : a^{(i)} = \min_{\substack{\text{periodic } \sigma(x) \\ \nabla \cdot \sigma(x) = 0 \\ \langle \sigma(x) \rangle = a^{(i)}}} \langle \sigma(x) : S(x) : \sigma(x) \rangle, \quad i = 1, 2, 3. \tag{12}$$

The effective compliance tensor $\boldsymbol{S}_*$ is equal to the inverse of the effective stiffness tensor $\boldsymbol{C}_* = (\boldsymbol{S}_*)^{-1}$. Indeed, the solution of the variational problem (9) with periodic strain fields results in a periodic stress field. Similarly, the solution of the problem (12) with periodic stress fields results in a periodic strain field. It immediately follows that the stiffness tensors relating average strain and stress fields for these problems are the same.

2.2. Dirichlet stiffness tensor

Let us solve problem (1) with three different affine (Dirichlet-type) boundary conditions

$$\boldsymbol{u}(\boldsymbol{x})|_\Gamma = \boldsymbol{a}^{(i)} \cdot \boldsymbol{x}|_\Gamma, \quad i = 1, 2, 3, \tag{13}$$

where Γ is the boundary of the unit square. One can check that the average strain tensors are equal to $\boldsymbol{a}^{(i)}$, $\bar{\boldsymbol{\varepsilon}}^{(i)} = \boldsymbol{a}^{(i)}$. A Dirichlet stiffness tensor $\boldsymbol{C}_\mathscr{D}$ of the cell can be introduced via the set of equations

$$\bar{\boldsymbol{\sigma}}^{(i)} = \boldsymbol{C}_\mathscr{D} : \bar{\boldsymbol{\varepsilon}}^{(i)}, \quad i = 1, 2, 3, \tag{14}$$

where $\bar{\boldsymbol{\sigma}}^{(i)}$ and $\bar{\boldsymbol{\varepsilon}}^{(i)}$ are the average stress and strain tensors defined as in (7) but for the Dirichlet-type boundary conditions (13). This tensor was introduced earlier by Huet (1990) who called it the kinematic apparent modulus tensor. The energy $W_\mathscr{D}(\bar{\boldsymbol{\varepsilon}}^{(i)})$ stored in the cell subject to the boundary conditions (13) is defined by

$$W_\mathscr{D}(\bar{\boldsymbol{\varepsilon}}^{(i)}) = \tfrac{1}{2} \langle \boldsymbol{\sigma}^{(i)}(\boldsymbol{x}) : \boldsymbol{\varepsilon}^{(i)}(\boldsymbol{x}) \rangle = \tfrac{1}{2} \bar{\boldsymbol{\sigma}}^{(i)} : \bar{\boldsymbol{\varepsilon}}^{(i)} = \tfrac{1}{2} \bar{\boldsymbol{\varepsilon}}^{(i)} : \boldsymbol{C}_\mathscr{D} : \bar{\boldsymbol{\varepsilon}}^{(i)}, \quad i = 1, 2, 3. \tag{15}$$

The Dirichlet stiffness tensor $\boldsymbol{C}_\mathscr{D}$ can be defined via the solution of the variational problems

$$\boldsymbol{a}^{(i)} : \boldsymbol{C}_\mathscr{D} : \boldsymbol{a}^{(i)} = \min_{\substack{\boldsymbol{\varepsilon}(\boldsymbol{x}) \\ \boldsymbol{\varepsilon}(\boldsymbol{x}) = \frac{1}{2}[\nabla \boldsymbol{u}(\boldsymbol{x}) + (\nabla \boldsymbol{u}(\boldsymbol{x}))^{\mathrm{T}}] \\ \boldsymbol{u}(\boldsymbol{x})|_\Gamma = \boldsymbol{a}^{(i)} \cdot \boldsymbol{x}|_\Gamma}} \langle \boldsymbol{\varepsilon}(\boldsymbol{x}) : \boldsymbol{C}(\boldsymbol{x}) : \boldsymbol{\varepsilon}(\boldsymbol{x}) \rangle, \quad i = 1, 2, 3. \tag{16}$$

Knowing the Dirichlet stiffness tensor allows one to find the energy $W_\mathscr{D}(\bar{\boldsymbol{\varepsilon}})$ and the average stresses $\boldsymbol{\sigma}$ in the unit square with any affine boundary conditions of the type $\boldsymbol{u}(\boldsymbol{x})|_\Gamma = \boldsymbol{\varepsilon} \cdot \boldsymbol{x}|_\Gamma$, by using the formulae

$$\bar{\boldsymbol{\sigma}} = \boldsymbol{C}_\mathscr{D} : \bar{\boldsymbol{\varepsilon}}, \quad W_\mathscr{D}(\bar{\boldsymbol{\varepsilon}}) = \tfrac{1}{2} \bar{\boldsymbol{\varepsilon}} : \boldsymbol{C}_\mathscr{D} : \bar{\boldsymbol{\varepsilon}}. \tag{17}$$

2.3. Neumann stiffness tensor

Consider the boundary-value problem (1) with uniform stress (Neumann-type) boundary conditions

$$\boldsymbol{\sigma}(\mathbf{x}) \cdot \boldsymbol{n}|_\Gamma = \boldsymbol{a}^{(i)} \cdot \boldsymbol{n}|_\Gamma, \quad i = 1, 2, 3, \tag{18}$$

where $\boldsymbol{n}$ is the outward normal unit vector. In this case, the average stress tensors $\bar{\boldsymbol{\sigma}}^{(i)}$

are equal to the tensors $\boldsymbol{a}^{(i)}$, i.e., $\bar{\boldsymbol{\sigma}}^{(i)} = \langle \boldsymbol{\sigma}^{(i)} \rangle = \boldsymbol{a}^{(i)}$. The Neumann compliance tensor $\boldsymbol{S}_{\mathcal{N}}$ is defined by the system

$$\bar{\boldsymbol{\varepsilon}}^{(i)} = \boldsymbol{S}_{\mathcal{N}} : \bar{\boldsymbol{\sigma}}^{(i)}, \quad i = 1, 2, 3, \tag{19}$$

with $\bar{\boldsymbol{\sigma}}^{(i)}$ and $\bar{\boldsymbol{\varepsilon}}^{(i)}$ being the average stress and strain tensors defined as in (7) for the Neumann-type boundary conditions (18). The energy $W_{\mathcal{N}}(\boldsymbol{\sigma}^{(i)})$ stored in the cell subject to the boundary conditions (18) is defined as

$$W_{\mathcal{N}}(\boldsymbol{\sigma}^{(i)}) = \tfrac{1}{2}\bar{\boldsymbol{\sigma}}^{(i)} : \bar{\boldsymbol{\varepsilon}}^{(i)} = \tfrac{1}{2}\bar{\boldsymbol{\sigma}}^{(i)} : \boldsymbol{S}_{\mathcal{N}} : \bar{\boldsymbol{\sigma}}^{(i)}, \quad i = 1, 2, 3. \tag{20}$$

The Neumann compliance tensor $\boldsymbol{S}_{\mathcal{N}}$ can be equivalently defined by the variational problems

$$\boldsymbol{a}^{(i)} : \boldsymbol{S}_{\mathcal{N}} : \boldsymbol{a}^{(i)} = \min_{\substack{\boldsymbol{\sigma}(\boldsymbol{x}) \\ \nabla \cdot \boldsymbol{\sigma}(\boldsymbol{x}) = 0 \\ \boldsymbol{\sigma}(\boldsymbol{x}) \cdot \boldsymbol{n}(\boldsymbol{x})|_{\Gamma} = \boldsymbol{a}^{(i)} \cdot \boldsymbol{n}(\boldsymbol{x})|_{\Gamma}}} \langle \boldsymbol{\sigma}(\boldsymbol{x}) : \boldsymbol{S}(\boldsymbol{x}) : \boldsymbol{\sigma}(\boldsymbol{x}) \rangle, \quad i = 1, 2, 3. \tag{21}$$

We denote the inverse of the compliance tensor $\boldsymbol{S}_{\mathcal{N}}$ as $\boldsymbol{C}_{\mathcal{N}} = (\boldsymbol{S}_{\mathcal{N}})^{-1}$ and name it the Neumann stiffness tensor. Huet (1990) called the same tensor the static apparent modulus tensor.

2.4. Numerical method for computing overall stiffness

To find the aforementioned overall stiffness tensors, one must solve the corresponding boundary-value elasticity problems. We compute elastic fields for the microstructures using the DYNAFLOW.v98 (Prevost, 1997) finite element solver. The microgeometry is discretized on a rectangular mesh, with each element being assigned a particular material phase. In all cases, the elementary cells are meshed using a 30×30 grid. For the examples involving larger unit squares comprised of several elementary cells, it is important to maintain the same mesh scale to ensure consistent results with no variation due to mesh size. Therefore, the composite in Fig. 1(b) would be meshed at 60×60 and so on.

The three types of analyses performed are distinguished by the imposed displacements and loads. In the case of Dirichlet conditions, displacements are imposed at the boundary corresponding to the affine boundary conditions (13). Similarly, for the Neumann conditions, distributed loads are imposed corresponding to the conditions (18). In both cases, average stress and strain tensors are computed over all of the elements in the mesh for each of the three fundamental tests

$$\mathbf{u}(\boldsymbol{x})|_{\Gamma} = \boldsymbol{a}^{(i)} \cdot \boldsymbol{x}|_{\Gamma} \quad \text{or} \quad \boldsymbol{\sigma} \cdot \boldsymbol{n}|_{\Gamma} = \boldsymbol{a}^{(i)} \cdot \boldsymbol{n}|_{\Gamma}, \quad i = 1, 2, 3, \tag{22}$$

from local field values provided by the finite element solver, where the $\boldsymbol{a}^{(i)}$ are given by (5). With these results, the Dirichlet and Neumann stiffness tensors may be computed from the relations (14) and (19), respectively.

To compute the effective properties of infinite media, it is useful to write the strain in a material as

$$\boldsymbol{\varepsilon}^{(i)}(\boldsymbol{x}) = \boldsymbol{\varepsilon}_0^{(i)} - \boldsymbol{\varepsilon}_F^{(i)}(\boldsymbol{x}), \quad i = 1, 2, 3, \tag{23}$$

where $\boldsymbol{\varepsilon}_0^{(i)}$ represents the given average strain over the domain of the unit square and $\boldsymbol{\varepsilon}_F^{(i)} = (\nabla \boldsymbol{u}_F^{(i)} + (\nabla \boldsymbol{u}_F^{(i)})^{\mathrm{T}})/2$ is the corresponding local fluctuation due to inhomogeneities. It has been shown (Bensoussan et al., 1978; Sanchez-Palencia, 1980) that the effective stiffness tensor may be written in energy form as

$$\boldsymbol{\varepsilon}_0^{(i)} : \boldsymbol{C}_* : \boldsymbol{\varepsilon}_0^{(j)} = \frac{1}{Y} \int_Y (\boldsymbol{\varepsilon}_0^{(i)} - \boldsymbol{\varepsilon}_F^{(i)}) : \boldsymbol{C} : (\boldsymbol{\varepsilon}_0^{(j)} - \boldsymbol{\varepsilon}_F^{(j)}) \, \mathrm{d}Y, \quad i, j = 1, 2, 3, \tag{24}$$

where $\boldsymbol{\varepsilon}_F^{(i)}$ satisfies

$$\int_Y \boldsymbol{\varepsilon}(\boldsymbol{v}) : \boldsymbol{C} : \boldsymbol{\varepsilon}_F^{(i)} \, \mathrm{d}Y = \int_Y \boldsymbol{\varepsilon}(\boldsymbol{v}) : \boldsymbol{C} : \boldsymbol{\varepsilon}_0^{(i)} \, \mathrm{d}Y,$$

$$\forall \boldsymbol{\varepsilon}(\boldsymbol{v}) = \frac{1}{2} [\nabla \boldsymbol{v}(\boldsymbol{x}) + (\nabla \boldsymbol{v}(\boldsymbol{x}))^{\mathrm{T}}], \quad \boldsymbol{v} \text{ is } Y \text{ periodic}, \tag{25}$$

for any periodic displacement trial field $\boldsymbol{v}$, where Y is the periodic cell (unit square in our case). Bourgat (1977) and Guedes and Kikuchi (1991) provide a means of numerically calculating the effective properties of infinite media using finite element methods by rewriting (24) in a discretized form

$$\boldsymbol{\varepsilon}_0^{(i)} : \boldsymbol{C}_* : \boldsymbol{\varepsilon}_0^{(j)} = \frac{1}{Y} \sum_{e=1}^{NE} \int_{Y_e} (\boldsymbol{\varepsilon}_0^{(i)} - \boldsymbol{\varepsilon}_{Fe}^{(i)})^{\mathrm{T}} : \boldsymbol{C}_e : (\boldsymbol{\varepsilon}_0^{(i)} - \boldsymbol{\varepsilon}_{Fe}^{(j)}) \, \mathrm{d}Y_e, \quad i, j = 1, 2, 3, \tag{26}$$

where $\boldsymbol{\varepsilon}_{Fe}^{(i)}$ is the field fluctuation in element e, $\boldsymbol{C}_e$ is the stiffness tensor of the material occupying element e and Y_e is the area of element e. The summation is performed over all of the NE elements in the finite element mesh. Performing the integration, we get

$$\boldsymbol{\varepsilon}_0^{(i)} : \boldsymbol{C}_* : \boldsymbol{\varepsilon}_0^{(j)} = \frac{1}{Y} \sum_{e=1}^{NE} (\{d_0\}^{(i)} - \{d_e\}^{(i)})^{\mathrm{T}} [s_e] (\{d_0\}^{(j)} - \{d_e\}^{(j)}), \quad i, j = 1, 2, 3, \tag{27}$$

where $\{d_e\}^{(i)} = [u_1^{(i)}, v_1^{(i)}, \ldots, u_4^{(i)}, v_4^{(i)}]$ is the finite element displacement vector of the four node linear elastic quadrilateral finite element, obtained from the finite element solver for the i fundamental test. The components $u_n^{(i)}$ and $v_n^{(i)}$ are the x and y displacements, respectively, of node n. The vector $\{d^0\}^{(i)}$ is the finite element displacement vector corresponding to the appropriate unit strain problem. The element stiffness matrix $[s_e]$ is defined as

$$[s_e] = \int_{Y_e} [B_e]^{\mathrm{T}} [C_e][B_e] \, \mathrm{d}Y_e, \tag{28}$$

where $[B_e]$ is the finite element strain–displacement matrix and the square brackets denote the matrix representation of the corresponding tensors.

The periodic boundary conditions for the fluctuating parts of the displacement

$$\boldsymbol{u}_F^{(i)}(0, y) = \boldsymbol{u}_F^{(i)}(1, y), \quad \forall y \in [0, 1],$$

$$u_F^{(i)}(x, 0) = u_F^{(i)}(x, 1), \quad \forall x \in [0, 1], \quad i = 1, 2, 3, \tag{29}$$

are enforced by assigning the same node number to opposing nodes of the finite element mesh. The unit square is constrained to prevent rigid body motion and the fundamental strains $\varepsilon_0^{(i)}$ are converted to the equivalent internal force vector $\{R\}^{(i)}$ by the relation

$$\{R\}^{(i)} = \sum_{e=1}^{NE} \int_{Y_e} [B_e]^{\mathrm{T}} [C_e][\varepsilon_0^{(i)}] \, \mathrm{d} Y_e. \tag{30}$$

The summation indicates the usual finite element assembly procedure. For a more detailed treatment of the numerical homogenization procedure, the reader is referred to the works cited earlier in this section.

3. One-scale composites

If the cell material is homogeneous, then the tensors $C_{\mathscr{D}}$, $C_{\mathscr{N}}$ and C_* are equal to each other and equal to the stiffness tensor of the homogeneous material. We will study a different situation where the unit square is composed of two distinct phases.

Consider the sequence of structures illustrated by Fig. 1. Figure 1(a) shows a unit
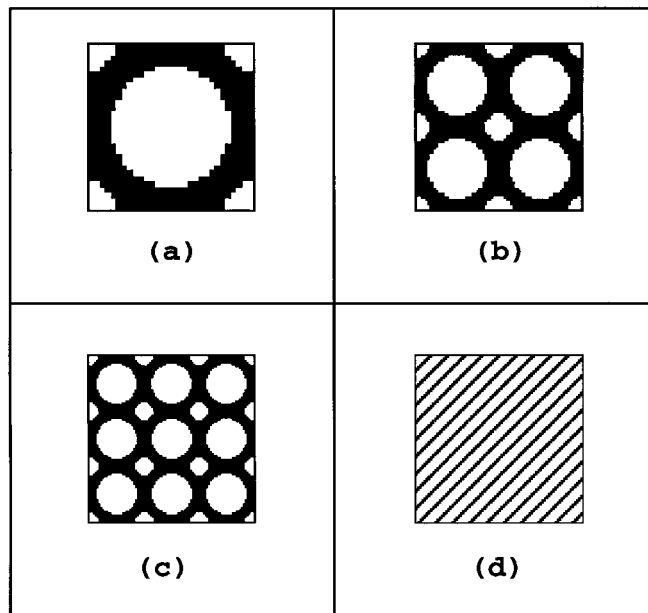
Fig. 1. Composite samples with different scale factors n. (a) shows an elementary cell of scale factor $n = 1$. (b) and (c) show unit squares composed of n^2 elementary cells, with $n = 2$ and $n = 3$, respectively. (d) symbolically represents the infinite system, $n = \infty$.

square filled with two elastic materials. We will treat this configuration as an elementary cell. This structure is then repeated in Figs 1(b)–(d). However, in these figures we scale the elementary cell by the factor $1/n$ and combine n^2 of such cells to form a unit square. For the structures depicted in Fig. 1(b) and (c), $n = 2$ and $n = 3$, respectively. Figure 1(d) symbolically depicts the limiting situation when $n \to \infty$. Obviously, the effective stiffness tensor is independent of the scale factor. However, the Dirichlet and Neumann stiffness tensors may depend on n. Our goal is to study this dependence.

3.1. Dependence of stiffness on scale factor

We will denote by superscript n the Dirichlet tensor $\boldsymbol{C}_{\mathcal{D}}^{(n)}$ of the structure with the scale factor n such that $\boldsymbol{C}_{\mathcal{D}}^{(1)}$, $\boldsymbol{C}_{\mathcal{D}}^{(2)}$, $\boldsymbol{C}_{\mathcal{D}}^{(3)}$ and $\boldsymbol{C}_{\mathcal{D}}^{(\infty)}$ correspond to the Dirichlet stiffness tensors of the unit squares shown in Figs 1(a)–(d), respectively. Similarly, we will denote by superscript n the Neumann compliance tensor $\boldsymbol{S}_{\mathcal{N}}^{(n)}$ and the Neumann stiffness tensor $\boldsymbol{C}_{\mathcal{N}}^{(n)} = (\boldsymbol{S}_{\mathcal{N}}^{(n)})^{-1}$ of the structure with the scale factor n.

The Dirichlet stiffness tensors with the scale factors that differ by an integral factor K satisfy the following inequalities (Huet, 1990)

$$\boldsymbol{C}_{\mathcal{D}}^{(n)} \geqslant \boldsymbol{C}_{\mathcal{D}}^{(Kn)} \geqslant \boldsymbol{C}_{\mathcal{D}}^{(\infty)}, \quad \forall \text{ integer } K, n. \tag{31}$$

Here it is understood that for two elastic tensors $\boldsymbol{A}$ and $\boldsymbol{B}$,

$$\boldsymbol{B} - \boldsymbol{A} \geqslant 0 \text{ is equivalent to } \boldsymbol{e} : (\boldsymbol{B} - \boldsymbol{A}) : \boldsymbol{e} \geqslant 0, \quad \forall \boldsymbol{e}, \tag{32}$$

where $\boldsymbol{e}$ is an arbitrary symmetric second-order tensor.

To prove (31) one can use the variational definition (16). Consider, for example, variational problems for samples with the scale factors n and Kn, respectively. Let $\boldsymbol{u}^{(n)}(\boldsymbol{x})$ be a solution of the former problem. One can then rescale this solution as $\boldsymbol{u}^{(n)}(K\boldsymbol{x})/K$ and combine K^2 such fields to use as a trial field for the sample with scale factor Kn. As a result, the first inequality in (31) immediately follows. One can continue in this manner to prove the second inequality in (31).

Similarly, by using the minimum complementary energy principle (21) one can prove (Huet, 1990) that

$$\boldsymbol{S}_{\mathcal{N}}^{(n)} \geqslant S_{\mathcal{N}}^{(Kn)} \geqslant \boldsymbol{S}_{\mathcal{N}}^{(\infty)}, \quad \forall \text{ integer } K, n. \tag{33}$$

Using the Neumann stiffness tensor $\boldsymbol{C}_{\mathcal{N}}^{(n)} = (\boldsymbol{S}_{\mathcal{N}}^{(n)})^{-1}$, we may rewrite (33) as

$$\boldsymbol{C}_{\mathcal{N}}^{(n)} \leqslant \boldsymbol{C}_{\mathcal{N}}^{(Kn)} \leqslant \boldsymbol{C}_{\mathcal{N}}^{(\infty)}, \quad \forall \text{ integer } K, n. \tag{34}$$

We may also expect that the following inequalities,

$$\boldsymbol{C}_{\mathcal{D}}^{(1)} \geqslant \boldsymbol{C}_{\mathcal{D}}^{(2)} \geqslant \boldsymbol{C}_{\mathcal{D}}^{(3)} \geqslant \cdots \geqslant \boldsymbol{C}_{\mathcal{D}}^{(\infty)}, \tag{35}$$

$$\boldsymbol{C}_{\mathcal{N}}^{(1)} \leqslant \boldsymbol{C}_{\mathcal{N}}^{(2)} \leqslant \boldsymbol{C}_{\mathcal{N}}^{(3)} \leqslant \cdots \leqslant \boldsymbol{C}_{\mathcal{N}}^{(\infty)}, \tag{36}$$

hold. The chains of the inequalities similar to (35) and (36) were first formulated by Ostoja-Starzewski (1993, 1996, 1998). However, the proof in the aforementioned

papers is incomplete and we were not able to verify it. We will demonstrate the validity of these inequalities numerically with several examples.

In the limiting case $n = \infty$ and finite contrast ratio of the phase properties, the composite material in the unit square displays homogeneous behavior (at the scale of the unit square) and the stiffness tensors $\boldsymbol{C}_{\mathscr{D}}^{(\infty)}$ and $\boldsymbol{C}_{\mathscr{N}}^{(\infty)}$ are equal and equal to the effective stiffness tensor $\boldsymbol{C}_*$, i.e., $\boldsymbol{C}_{\mathscr{N}}^{(\infty)} = \boldsymbol{C}_* = \boldsymbol{C}_{\mathscr{D}}^{(\infty)}$.

3.2. Bounds on the overall stiffness

There is an extensive literature dealing with bounds on the effective properties of elastic materials (see, e.g., reviews by Hashin, 1993; Willis, 1977). The simplest ones are given by the arithmetic and harmonic means of the phase properties (Hill, 1952), i.e.,

$$\langle \boldsymbol{C}^{-1} \rangle^{-1} \leqslant \boldsymbol{C}_* \leqslant \langle \boldsymbol{C} \rangle. \tag{37}$$

By using constant trial fields in the variational principles (16) and (21), one can easily show that the Dirichlet and Neumann stiffness tensors satisfy these inequalities (see also Huet, 1990 for an alternative proof). For isotropic stiffness tensors of two-phase composites these bounds can be written in terms of the bounds on the bulk and shear moduli

$$\kappa_h \leqslant \kappa_{\mathscr{N}} \leqslant \kappa_* \leqslant \kappa_{\mathscr{D}} \leqslant \kappa_a, \quad \mu_h \leqslant \mu_{\mathscr{N}} \leqslant \mu_* \leqslant \mu_{\mathscr{D}} \leqslant \mu_a, \tag{38}$$

where $\kappa_{\mathscr{D}}, \mu_{\mathscr{D}}$ and $\kappa_{\mathscr{N}}, \mu_{\mathscr{N}}$ are the bulk and shear moduli of the Dirichlet and Neumann stiffness tensors, respectively. Here

$$\kappa_h = [f_1 \kappa_1^{-1} + f_2 \kappa_2^{-1}]^{-1}, \quad \kappa_a = f_1 \kappa_1 + f_2 \kappa_2,$$

$$\mu_h = [f_1 \mu_1^{-1} + f_2 \mu_2^{-1}]^{-1}, \quad \mu_a = f_1 \mu_1 + f_2 \mu_2, \tag{39}$$

where f_1 and $f_2 = 1 - f_1$ are the phase volume fractions. The bounds (37) are simple but too wide in most cases.

More restrictive bounds on the effective properties of isotropic two-dimensional composites were found by Hashin (1965) by using the Hashin and Shtrikman (1963) variational method. The bounds can be presented as the two-sided inequalities

$$\kappa_{HS}^L \leqslant \kappa_* \leqslant \kappa_{HS}^U, \quad \mu_{HS}^L \leqslant \mu_* \leqslant \mu_{HS}^U, \tag{40}$$

where (for well-ordered phases with $\kappa_1 \geqslant \kappa_2$ and $\mu_1 \geqslant \mu_2$)

$$\kappa_{HS}^L = f_1 \kappa_1 + f_2 \kappa_2 - \frac{f_1 f_2 (\kappa_1 - \kappa_2)^2}{f_2 \kappa_1 + f_1 \kappa_2 + \mu_2}, \tag{41}$$

$$\kappa_{HS}^U = f_1 \kappa_1 + f_2 \kappa_2 - \frac{f_1 f_2 (\kappa_1 - \kappa_2)^2}{f_2 \kappa_1 + f_1 \kappa_2 + \mu_1}, \tag{42}$$

$$\mu_{HS}^L = f_1 \mu_1 + f_2 \mu_2 - \frac{f_1 f_2 (\mu_1 - \mu_2)^2}{f_2 \mu_1 + f_1 \mu_2 + \kappa_2 \mu_2 / (\kappa_2 + 2\mu_2)}, \tag{43}$$

$$\mu_{HS}^U = f_1\mu_1 + f_2\mu_2 - \frac{f_1f_2(\mu_1 - \mu_2)^2}{f_2\mu_1 + f_1\mu_2 + \kappa_1\mu_1/(\kappa_1 + 2\mu_1)}. \tag{44}$$

Obviously, the Hashin–Shtrikman lower bounds are also bounds for the Dirichlet stiffness tensor. Similarly, the Hashin–Shtrikman upper bounds restrict the Neumann stiffness tensor from above. However, at the moment there are no upper bounds on the Dirichlet moduli that are sharper than the arithmetic mean bound and no lower bounds on the Neumann moduli that are sharper than the harmonic mean bounds. Moreover, these rather simple bounds are obviously optimal if one is allowed to divide the composite into the smaller and smaller pieces as in the Huet (1990) approach. On the contrary, in our problem we restrict the smallest admissible size of the sample by the size of the periodic cell. Thus, it should be possible to obtain more precise bounds on the Dirichlet and Neumann stiffness tensor. The Hashin–Shtrikman bounds (40) that are optimal for the infinite composite system, are the natural candidates for such bounds. We will check (numerically) whether Dirichlet and Neumann bulk and shear moduli satisfy the Hashin–Shtrikman bounds (40).

Below is the summary of our theoretical discussion:

- For any integers K, n,

$$\langle \boldsymbol{C}^{-1} \rangle^{-1} \leqslant \boldsymbol{C}_{\mathcal{N}}^{(n)} \leqslant \boldsymbol{C}_{\mathcal{N}}^{(Kn)} \leqslant \boldsymbol{C}_{\mathcal{N}}^{(\infty)} = \boldsymbol{C}_* = \boldsymbol{C}_{\mathcal{D}}^{(\infty)} \leqslant \boldsymbol{C}_{\mathcal{D}}^{(Kn)} \leqslant \boldsymbol{C}_{\mathcal{D}}^{(n)} \leqslant \langle \boldsymbol{C} \rangle. \tag{45}$$

  This chain of inequalities was first proven by Huet (1990).

- We expect the chain of inequalities

$$\boldsymbol{C}_{\mathcal{N}}^{(1)} \leqslant \boldsymbol{C}_{\mathcal{N}}^{(2)} \leqslant \boldsymbol{C}_{\mathcal{N}}^{(3)} \leqslant \cdots \leqslant \boldsymbol{C}_{\mathcal{N}}^{(\infty)} = \boldsymbol{C}_* = \boldsymbol{C}_{\mathcal{D}}^{(\infty)} \leqslant \cdots \leqslant \boldsymbol{C}_{\mathcal{D}}^{(3)} \leqslant \boldsymbol{C}_{\mathcal{D}}^{(2)} \leqslant \boldsymbol{C}_{\mathcal{D}}^{(1)} \tag{46}$$

  to hold. We will check these inequalities numerically.

- At the moment, there are neither analogues of the Hashin–Shtrikman upper bound for the Dirichlet stiffness tensor nor analogues of the Hashin–Shtrikman lower bound for the Neumann stiffness tensor. We would like to check numerically whether the first and the last inequalities in the chains

$$\kappa_{HS}^L \leqslant \kappa_{\mathcal{N}} \leqslant \kappa_* \leqslant \kappa_{\mathcal{D}} \leqslant \kappa_{HS}^U, \quad \mu_{HS}^L \leqslant \mu_{\mathcal{N}} \leqslant \mu_* \leqslant \mu_{\mathcal{D}} \leqslant \mu_{HS}^U \tag{47}$$

  hold true.

3.3. Numerical experiments

Our goal now is to check the theoretical results numerically and study the rate of convergence of the Dirichlet and Neumann stiffness tensors to the effective tensor $\boldsymbol{C}_*$ for increasing scale factor n. We study three different elementary cells shown in Fig. 2. The black regions in the figure correspond to the stiff phase 1, the white regions correspond to the compliant phase 2.

The first cell shown in Fig. 2(a) corresponds to the isotropic two-phase composite with effective bulk modulus close to the Hashin (1965) upper bound (42). This represents an example of a stiff matrix composite with a rigid matrix and compliant inclusions. The second cell shown in Fig. 2(b) corresponds to an isotropic two-phase composite having an effective bulk modulus that is close to the Hashin (1965) lower
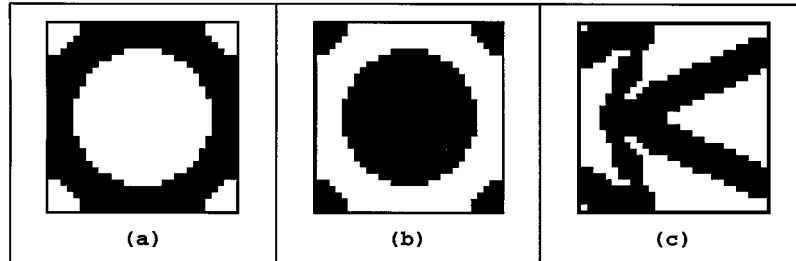
Fig. 2. Three different elementary cells. (a) corresponds to the stiff composite with effective bulk modulus close to the Hashin (1965) upper bound. (b) corresponds to the compliant composite with effective bulk modulus close to the Hashin (1965) lower bound. (c) corresponds to the nearly isotropic composite with negative Poisson's ratio.

bound (41). This is an example of a compliant matrix microstructure with a compliant matrix and stiff inclusions. Note that the structures in Figs 2(a) and (b) differ solely by interchanging the position of the stiff and compliant phases, preserving the micro-geometry. Finally, the third cell shown in Fig. 2(c) corresponds to a nearly isotropic composite with negative Poisson's ratio. This represents an example of a material with rather unusual mechanical properties. Although we cannot exhaust all of the possible microstructures by studying only these three examples, we believe this set is very representative.

We study numerically the Dirichlet and Neumann problems with the scale factor n ranging from 1–6 and the periodic problem which corresponds to scale factor $n = \infty$. First, we will study two-phase composites with the contrast ratio between the phase properties equal to $E_1/E_2 = 10$, i.e., with the moduli and volume fractions

$$E_1 = 10.0, \quad E_2 = 1.0, \quad v_1 = v_2 = 0.3, \quad f_1 = f_2 = 0.5. \tag{48}$$

The phase bulk and shear moduli are determined by relations (3) yielding

$$\kappa_1 = 7.14, \quad \mu_1 = 3.85, \quad \kappa_2 = 0.714, \quad \mu_2 = 0.385. \tag{49}$$

For these phase moduli and volume fractions, the bulk and moduli bounds are given by

$$\kappa_h = 1.30, \quad \kappa_{HS}^L = 1.53, \quad \kappa_{HS}^U = 2.60, \quad \kappa_a = 3.92, \tag{50}$$

$$\mu_h = 0.70, \quad \mu_{HS}^L = 0.814, \quad \mu_{HS}^U = 1.36, \quad \mu_a = 2.12. \tag{51}$$

We will then investigate composites with phase moduli and volume fractions

$$E_1 = 1000.0, \quad E_2 = 1.0, \quad v_1 = v_2 = 0.3, \quad f_1 = f_2 = 0.5, \tag{52}$$

$$\kappa_1 = 714.0, \quad \mu_1 = 385.0, \quad \kappa_2 = 0.714, \quad \mu_2 = 0.385, \tag{53}$$

resulting in the bounds

$$\kappa_h = 1.43, \quad \kappa_{HS}^L = 1.81, \quad \kappa_{HS}^U = 186.0, \quad \kappa_a = 357.4, \tag{54}$$

$$\mu_h = 0.769, \quad \mu_{HS}^L = 0.954, \quad \mu_{HS}^U = 94.84, \quad \mu_a = 192.7. \tag{55}$$

The results of our numerical experiments for the one-scale composites are shown in Tables 1–5. The first column of each of these tables shows the microstructures of five composite samples with scale factors one, two, three, six and infinity, respectively.

Table 1
Results for one-scale maximum bulk modulus microstructure with a contrast ratio of $E_1/E_2 = 10$. Stiffness values are given in full tensor form followed by the moduli, κ, μ^I and μ^{II}, respectively
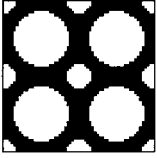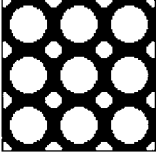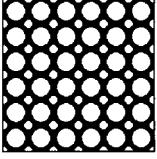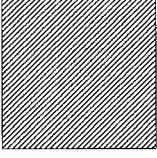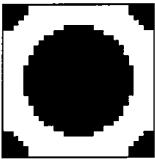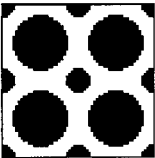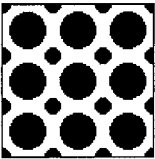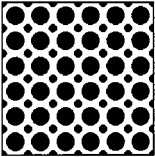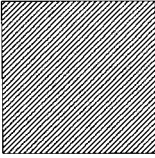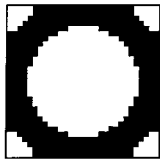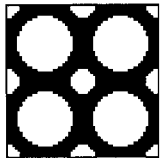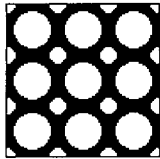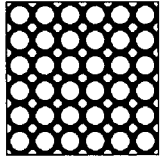
Unit Square	Dirichlet	Neumann
	$\begin{bmatrix} 4.08 & 1.14 & 0.0 \\ 1.14 & 4.08 & 0.0 \\ 0.0 & 0.0 & 1.52 \end{bmatrix}$ $\begin{bmatrix} 2.61 & 1.47 & 1.52 \end{bmatrix}$	$\begin{bmatrix} 3.12 & 1.48 & 0.0 \\ 1.48 & 3.12 & 0.0 \\ 0.0 & 0.0 & 0.93 \end{bmatrix}$ $\begin{bmatrix} 2.30 & 0.82 & 0.93 \end{bmatrix}$
	$\begin{bmatrix} 3.93 & 1.25 & 0.0 \\ 1.25 & 3.93 & 0.0 \\ 0.0 & 0.0 & 1.35 \end{bmatrix}$ $\begin{bmatrix} 2.59 & 1.34 & 1.35 \end{bmatrix}$	$\begin{bmatrix} 3.39 & 1.42 & 0.0 \\ 1.42 & 3.39 & 0.0 \\ 0.0 & 0.0 & 1.02 \end{bmatrix}$ $\begin{bmatrix} 2.41 & 0.99 & 1.02 \end{bmatrix}$
	$\begin{bmatrix} 3.87 & 1.29 & 0.0 \\ 1.29 & 3.87 & 0.0 \\ 0.0 & 0.0 & 1.29 \end{bmatrix}$ $\begin{bmatrix} 2.58 & 1.29 & 1.29 \end{bmatrix}$	$\begin{bmatrix} 3.50 & 1.40 & 0.0 \\ 1.40 & 3.50 & 0.0 \\ 0.0 & 0.0 & 1.07 \end{bmatrix}$ $\begin{bmatrix} 2.45 & 1.05 & 1.07 \end{bmatrix}$
	$\begin{bmatrix} 3.82 & 1.33 & 0.0 \\ 1.33 & 3.82 & 0.0 \\ 0.0 & 0.0 & 1.24 \end{bmatrix}$ $\begin{bmatrix} 2.58 & 1.25 & 1.24 \end{bmatrix}$	$\begin{bmatrix} 3.62 & 1.38 & 0.0 \\ 1.38 & 3.62 & 0.0 \\ 0.0 & 0.0 & 1.12 \end{bmatrix}$ $\begin{bmatrix} 2.50 & 1.12 & 1.12 \end{bmatrix}$
	$\begin{bmatrix} 3.76 & 1.37 & 0.0 \\ 1.37 & 3.76 & 0.0 \\ 0.0 & 0.0 & 1.19 \end{bmatrix}$ $\begin{bmatrix} 2.57 & 1.20 & 1.19 \end{bmatrix}$	$\begin{bmatrix} 3.76 & 1.37 & 0.0 \\ 1.37 & 3.76 & 0.0 \\ 0.0 & 0.0 & 1.19 \end{bmatrix}$ $\begin{bmatrix} 2.57 & 1.20 & 1.19 \end{bmatrix}$

Table 2

Results for one-scale minimum bulk modulus microstructure with a contrast ratio of $E_1/E_2 = 10$. Stiffness values are given in full tensor form followed by the moduli κ, μ^{I} and μ^{II}, respectively
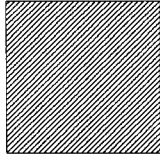
Unit Square	Dirichlet	Neumann
	$\begin{bmatrix} 2.69 & 0.72 & 0.0 \\ 0.72 & 2.69 & 0.0 \\ 0.0 & 0.0 & 1.03 \end{bmatrix}$ $\begin{bmatrix} 1.71 & 0.99 & 1.03 \end{bmatrix}$	$\begin{bmatrix} 2.31 & 0.78 & 0.0 \\ 0.78 & 2.31 & 0.0 \\ 0.0 & 0.0 & 0.79 \end{bmatrix}$ $\begin{bmatrix} 1.55 & 0.77 & 0.79 \end{bmatrix}$
	$\begin{bmatrix} 2.59 & 0.70 & 0.0 \\ 0.70 & 2.59 & 0.0 \\ 0.0 & 0.0 & 0.94 \end{bmatrix}$ $\begin{bmatrix} 1.65 & 0.95 & 0.94 \end{bmatrix}$	$\begin{bmatrix} 2.37 & 0.75 & 0.0 \\ 0.75 & 2.37 & 0.0 \\ 0.0 & 0.0 & 0.83 \end{bmatrix}$ $\begin{bmatrix} 1.56 & 0.81 & 0.83 \end{bmatrix}$
	$\begin{bmatrix} 2.52 & 0.70 & 0.0 \\ 0.70 & 2.52 & 0.0 \\ 0.0 & 0.0 & 0.92 \end{bmatrix}$ $\begin{bmatrix} 1.61 & 0.91 & 0.92 \end{bmatrix}$	$\begin{bmatrix} 2.39 & 0.73 & 0.0 \\ 0.73 & 2.39 & 0.0 \\ 0.0 & 0.0 & 0.84 \end{bmatrix}$ $\begin{bmatrix} 1.56 & 0.83 & 0.84 \end{bmatrix}$
	$\begin{bmatrix} 2.47 & 0.70 & 0.0 \\ 0.70 & 2.47 & 0.0 \\ 0.0 & 0.0 & 0.89 \end{bmatrix}$ $\begin{bmatrix} 1.59 & 0.89 & 0.89 \end{bmatrix}$	$\begin{bmatrix} 2.41 & 0.72 & 0.0 \\ 0.72 & 2.41 & 0.0 \\ 0.0 & 0.0 & 0.85 \end{bmatrix}$ $\begin{bmatrix} 1.57 & 0.85 & 0.85 \end{bmatrix}$
	$\begin{bmatrix} 2.43 & 0.71 & 0.0 \\ 0.71 & 2.43 & 0.0 \\ 0.0 & 0.0 & 0.89 \end{bmatrix}$ $\begin{bmatrix} 1.57 & 0.86 & 0.89 \end{bmatrix}$	$\begin{bmatrix} 2.43 & 0.71 & 0.0 \\ 0.71 & 2.43 & 0.0 \\ 0.0 & 0.0 & 0.89 \end{bmatrix}$ $\begin{bmatrix} 1.57 & 0.86 & 0.89 \end{bmatrix}$

The second column gives the Dirichlet stiffness tensor computed using affine boundary conditions on the corresponding structures. The third column shows the same results for Neumann conditions.

The stiffness tensor is given in two equivalent forms. First, we show the full matrix

Table 3
Results for one-scale maximum bulk modulus microstructure with a contrast ratio of $E_1/E_2 = 1000$. Stiffness values are given in full tensor form followed by the moduli κ, μ^{I} and μ^{II}, respectively
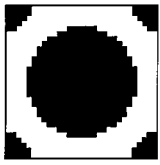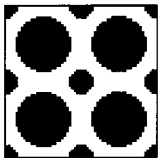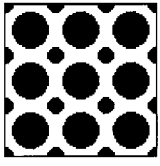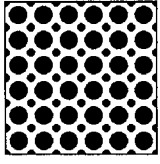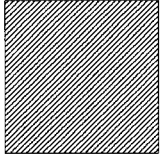
Unit Square	Dirichlet	Neumann
	$\begin{bmatrix} 288.82 & 81.25 & 0.0 \\ 81.25 & 288.82 & 0.0 \\ 0.0 & 0.0 & 114.61 \end{bmatrix}$ $\begin{bmatrix} 185.04 & 103.79 & 114.61 \end{bmatrix}$	$\begin{bmatrix} 14.78 & 6.38 & 0.0 \\ 6.38 & 14.78 & 0.0 \\ 0.0 & 0.0 & 6.69 \end{bmatrix}$ $\begin{bmatrix} 10.58 & 4.20 & 6.69 \end{bmatrix}$
	$\begin{bmatrix} 266.17 & 98.05 & 0.0 \\ 98.05 & 266.17 & 0.0 \\ 0.0 & 0.0 & 80.99 \end{bmatrix}$ $\begin{bmatrix} 182.11 & 84.06 & 80.99 \end{bmatrix}$	$\begin{bmatrix} 27.12 & 7.74 & 0.0 \\ 7.74 & 27.12 & 0.0 \\ 0.0 & 0.0 & 10.05 \end{bmatrix}$ $\begin{bmatrix} 17.43 & 9.69 & 10.05 \end{bmatrix}$
	$\begin{bmatrix} 258.03 & 104.29 & 0.0 \\ 104.29 & 258.03 & 0.0 \\ 0.0 & 0.0 & 69.09 \end{bmatrix}$ $\begin{bmatrix} 181.16 & 76.87 & 69.09 \end{bmatrix}$	$\begin{bmatrix} 38.18 & 9.74 & 0.0 \\ 9.74 & 38.18 & 0.0 \\ 0.0 & 0.0 & 13.07 \end{bmatrix}$ $\begin{bmatrix} 23.96 & 14.22 & 13.07 \end{bmatrix}$
	$\begin{bmatrix} 249.70 & 110.67 & 0.0 \\ 110.67 & 249.70 & 0.0 \\ 0.0 & 0.0 & 57.52 \end{bmatrix}$ $\begin{bmatrix} 180.19 & 69.52 & 57.52 \end{bmatrix}$	$\begin{bmatrix} 65.19 & 16.53 & 0.0 \\ 16.53 & 65.19 & 0.0 \\ 0.0 & 0.0 & 19.84 \end{bmatrix}$ $\begin{bmatrix} 40.86 & 24.33 & 19.84 \end{bmatrix}$
	$\begin{bmatrix} 241.22 & 117.23 & 0.0 \\ 117.23 & 241.22 & 0.0 \\ 0.0 & 0.0 & 47.27 \end{bmatrix}$ $\begin{bmatrix} 179.23 & 62.00 & 47.27 \end{bmatrix}$	$\begin{bmatrix} 241.22 & 117.23 & 0.0 \\ 117.23 & 241.22 & 0.0 \\ 0.0 & 0.0 & 47.27 \end{bmatrix}$ $\begin{bmatrix} 179.23 & 62.00 & 47.27 \end{bmatrix}$

$$C = \begin{bmatrix} C_{1111} & C_{1122} & 0 \\ C_{1122} & C_{2222} & 0 \\ 0 & 0 & C_{1212} \end{bmatrix} \tag{56}$$

which consists of the components C_{ijkl} of the stiffness tensor for an orthotropic material.

Table 4
Results for one-scale minimum bulk modulus microstructure with a contrast ratio of $E_1/E_2 = 1000$. Stiffness values are given in full tensor form followed by the moduli κ, μ^{I} and μ^{II}, respectively
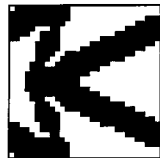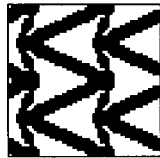
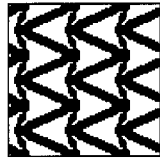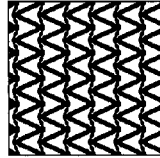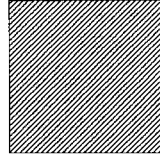| Unit Square	Dirichlet	Neumann
	$\begin{bmatrix} 36.92 & 9.10 & 0.0 \\ 9.10 & 36.92 & 0.0 \\ 0.0 & 0.0 & 23.18 \end{bmatrix}$ $\begin{bmatrix} 23.01 & 13.91 & 23.18 \end{bmatrix}$	$\begin{bmatrix} 2.73 & 0.97 & 0.0 \\ 0.97 & 2.73 & 0.0 \\ 0.0 & 0.0 & 0.93 \end{bmatrix}$ $\begin{bmatrix} 1.85 & 0.88 & 0.93 \end{bmatrix}$
	$\begin{bmatrix} 19.32 & 2.87 & 0.0 \\ 2.88 & 19.32 & 0.0 \\ 0.0 & 0.0 & 6.68 \end{bmatrix}$ $\begin{bmatrix} 11.10 & 8.23 & 6.68 \end{bmatrix}$	$\begin{bmatrix} 2.84 & 0.90 & 0.0 \\ 0.90 & 2.84 & 0.0 \\ 0.0 & 0.0 & 1.00 \end{bmatrix}$ $\begin{bmatrix} 1.87 & 0.97 & 1.00 \end{bmatrix}$
	$\begin{bmatrix} 13.72 & 1.73 & 0.0 \\ 1.73 & 13.72 & 0.0 \\ 0.0 & 0.0 & 3.60 \end{bmatrix}$ $\begin{bmatrix} 7.73 & 6.00 & 3.60 \end{bmatrix}$	$\begin{bmatrix} 2.88 & 0.87 & 0.0 \\ 0.87 & 2.88 & 0.0 \\ 0.0 & 0.0 & 1.03 \end{bmatrix}$ $\begin{bmatrix} 1.88 & 1.01 & 1.03 \end{bmatrix}$
	$\begin{bmatrix} 8.27 & 1.04 & 0.0 \\ 1.05 & 8.27 & 0.0 \\ 0.0 & 0.0 & 1.74 \end{bmatrix}$ $\begin{bmatrix} 4.66 & 3.62 & 1.74 \end{bmatrix}$	$\begin{bmatrix} 2.91 & 0.85 & 0.0 \\ 0.85 & 2.91 & 0.0 \\ 0.0 & 0.0 & 1.06 \end{bmatrix}$ $\begin{bmatrix} 1.88 & 1.03 & 1.06 \end{bmatrix}$
	$\begin{bmatrix} 2.95 & 0.83 & 0.0 \\ 0.83 & 2.95 & 0.0 \\ 0.0 & 0.0 & 1.10 \end{bmatrix}$ $\begin{bmatrix} 1.89 & 1.06 & 1.10 \end{bmatrix}$	$\begin{bmatrix} 2.95 & 0.83 & 0.0 \\ 0.83 & 2.95 & 0.0 \\ 0.0 & 0.0 & 1.10 \end{bmatrix}$ $\begin{bmatrix} 1.89 & 1.06 & 1.10 \end{bmatrix}$

For the examples in Tables 1–4, $C_{1111} = C_{2222}$ and we also give the bulk and two shear moduli of this matrix $[\kappa, \mu^{\mathrm{I}}, \mu^{\mathrm{II}}]$ computed as

$$\kappa = (C_{1111} + C_{1122})/2, \quad \mu^{\mathrm{I}} = (C_{1111} - C_{1122})/2, \quad \mu^{\mathrm{II}} = C_{1212}. \tag{57}$$

Notice that the Dirichlet and Neumann stiffness tensors satisfy the inequalities (46).

Table 5
Results for one-scale negative Poisson's ratio microstructure with a constant ratio $E_1/E_2 = 1000$. Stiffness values are given in full tensor form

Unit Square	Dirichlet	Neumann
	$\begin{bmatrix} 122.34 & -17.29 & 0.0 \\ -17.29 & 104.63 & 0.0 \\ 0.0 & 0.0 & 54.86 \end{bmatrix}$	$\begin{bmatrix} 5.76 & 0.57 & 0.0 \\ 0.57 & 5.35 & 0.0 \\ 0.0 & 0.0 & 1.75 \end{bmatrix}$
	$\begin{bmatrix} 85.65 & -28.41 & 0.0 \\ -28.41 & 80.35 & 0.0 \\ 0.0 & 0.0 & 49.10 \end{bmatrix}$	$\begin{bmatrix} 9.97 & 0.13 & 0.0 \\ 0.13 & 8.80 & 0.0 \\ 0.0 & 0.0 & 2.85 \end{bmatrix}$
	$\begin{bmatrix} 76.24 & -30.61 & 0.0 \\ -30.61 & 72.83 & 0.0 \\ 0.0 & 0.0 & 47.60 \end{bmatrix}$	$\begin{bmatrix} 13.45 & -0.73 & 0.0 \\ -0.73 & 12.21 & 0.0 \\ 0.0 & 0.0 & 3.97 \end{bmatrix}$
	$\begin{bmatrix} 68.30 & -32.01 & 0.0 \\ -32.01 & 65.62 & 0.0 \\ 0.0 & 0.0 & 46.45 \end{bmatrix}$	$\begin{bmatrix} 21.39 & -3.97 & 0.0 \\ -3.97 & 20.35 & 0.0 \\ 0.0 & 0.0 & 7.13 \end{bmatrix}$
	$\begin{bmatrix} 61.91 & -32.54 & 0.0 \\ -32.54 & 58.78 & 0.0 \\ 0.0 & 0.0 & 45.77 \end{bmatrix}$	$\begin{bmatrix} 61.91 & -32.54 & 0.0 \\ -32.54 & 58.78 & 0.0 \\ 0.0 & 0.0 & 45.77 \end{bmatrix}$

However, these inequalities should be understood in the sense of tensors as in (32). They may not be valid for the off-diagonal coefficients, as can be seen from the results for the C_{1122} components.

Table 1 summarizes results for the stiff matrix cell with moderate contrast ratio $E_1/E_2 = 10$ and phase moduli given by (48). For this structure, the Dirichlet stiffness tensor $C_{\mathscr{D}}^{(1)}$ (for the composite with a scale factor of 1) overestimates the effective tensor C_* with the largest difference of 28% for the shear modulus and 1.5% for the bulk modulus. This difference decreases sharply with n and for $n = 3$ does not exceed 8.5% for the shear modulus and 0.4% for the bulk modulus. This indicates that, for practical purposes, it is sufficient in this example to have a scale factor of 3 or higher to replace the non-homogeneous composite by the equivalent homogeneous material with the moduli given by homogenization theory. The Neumann stiffness tensors show greater variation from the effective stiffness tensor. This is explained by the fact that application of the force to the compliant phase leads to high deformations in this phase near the boundary. This results in higher average strain and smaller elastic moduli of the Neumann stiffness tensor. Comparing the stiffness tensors for the homogeneous displacement and homogeneous stress boundary conditions we see that the former much more closely resembles the deformation field in the cell with periodic boundary conditions.

Table 2 gives data for the compliant matrix composite cell (isotropic with minimum bulk modulus) with the same phase moduli. One can see that in this case the Neumann stiffness tensor more closely corresponds to the effective properties of the composite (i.e., to the result for periodic boundary conditions). This is because the homogeneous displacement boundary conditions induce strains in the stiff material near the boundary of the unit square that are significantly higher than those resulting from periodic boundary conditions.

Table 3 describes the results for the stiff matrix composite with high-contrast ratio (52). As we see, this results in a much greater difference between the effective properties and the Dirichlet and Neumann stiffness tensors. Even at the scale factor $n = 6$, the difference between the shear moduli μ^{II} of the Dirichlet stiffness tensor $C_{\mathscr{D}}^{(6)}$ and effective stiffness tensor C_* is around 20% (Table 3), although the bulk moduli differ by less than 0.5%. The Neumann stiffness of this composite is much smaller than the effective stiffness.

For the compliant matrix composite with high-contrast ratio (52) (Table 4), the Neumann stiffness tensor gives a reasonable approximation of the effective properties. The difference in the shear moduli is around 15% for the scale factor $n = 3$ and reduces to 4% for the scale factor $n = 6$. The difference in the bulk modulus is approximately 0.5%. The Dirichlet stiffness is much larger than the effective stiffness even for $n = 6$.

Table 5 summarizes results for the negative Poisson's ratio elementary cell (Fig. 2(c)) for the high-contrast ratio. Again, high phase contrast results in a much greater difference between the effective properties and the Dirichlet and Neumann stiffness tensors. Indeed, here the maximum difference in the stiffness moduli is on the order of 100% for $n = 1$. This clearly indicates that such microstructures cannot be described by the effective moduli if the size of the sample is comparable to the size of the elementary cell. For $n = 3$ the difference is on the order of 60% for the bulk modulus and 15% for the shear. Note that here the difference for hydrostatic compression is much higher than for the shear moduli. For $n = 6$, the results for Dirichlet conditions
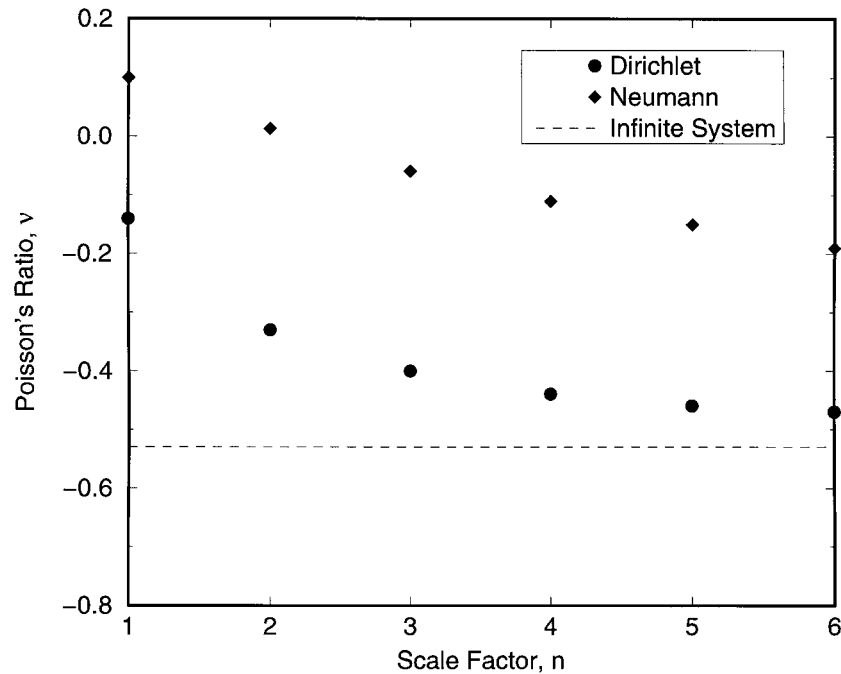
Fig. 3. Convergence of the Dirichlet and Neumann Poisson's ratios for the negative Poisson's ratio microstructure with increasing scale factor n in which $E_1/E_2 = 1000$.

are improved, not exceeding 25% error for the bulk and only 7% for the shear. However, the results for the Neumann conditions are still very far off. Figure 3 illustrates the convergence of the numerically computed Poisson's ratio $v = C_{1122}/C_{1111}$ for this example.

The results of Tables 1–5 demonstrate that the apparent tensors for the considered examples satisfy the inequalities (45) derived by Huet (1990), as well as the inequalities (46).

It is interesting to compare our conclusions with the results of Drugan and Willis (1996). They estimated, in particular, the minimum size of the representative volume element (RVE) for a material composed of a matrix either reinforced by strong spherical particles or weakened by spherical pores. The RVE was defined as the minimum characteristic wavelength of the average field fluctuations that still allowed for the description of the mean fields in the composite by the effective property tensor. They concluded (for models with microstructures that are roughly similar to our stiff and compliant composites) that the size of the RVE is on the order of two diameters of the reinforcing particles. This differs from our conclusion that even a composite with scale factor $n = 6$ and high contrast ratio may show large variation between the Dirichlet, Neumann and the effective properties tensors. These results do not contradict each other because of the difference between the problems studied. Indeed, we require the local strain or the local stress fields (on the boundary) to have prescribed

values, whereas Drugan and Willis (1996) considered variation of only the average fields. For example, prescribing an affine displacement on the 'strong' part of the boundary corresponds to a very high stored energy, whereas prescribing average strains in the region surrounding a stiff inclusion does not impose local strain in the stiff phase; this corresponds to a much lower energy level that is more comparable with periodic conditions.

Our results estimate finite-size effects for the composite sample, i.e., the influence of boundary effects on the overall energy of the sample. Thus, our more conservative estimates may be used to determine how large a composite sample should be compared to the size of the periodic cell in order to use the effective property tensor description. On the other hand, the less demanding estimates of Drugan and Willis (1996) may be sufficient to account for the scale effect associated with smooth variations of the average fields. Another possible explanation for the observed differences is that Drugan and Willis (1996) considered the full three-dimensional problem, whereas we studied two-dimensional models.

Another meaningful comparison can be made with the recent numerical results of Ostoja-Starzewski (1998) who considered the two-dimensional anti-plane shear problem for random composites. He also observed that the Dirichlet stiffness of the composite was a better approximation for the effective stiffness of a composite with a stiff matrix and compliant inclusions, whereas the Neumann stiffness better approximated the effective stiffness of a composite with a compliant matrix and stiff inclusions. His estimates of the RVE were somewhat larger than in our calculations. This may be explained by the difference in the problems (anti-plane shear vs two-dimensional elasticity) and a higher phase-contrast ratio in his calculations.

Summarizing our study of one-scale composites, we formulate the following conclusions:

- For matrix composites with a stiff matrix, compliant inclusions and a moderate phase contrast, the effective stiffness tensor is close to the Dirichlet stiffness tensor for structures with a scale factor of 3 or higher. The Neumann stiffness tensor underestimates the effective stiffness, even for a scale factor $n = 6$ by about 7%.
- For matrix composites with a compliant matrix, stiff inclusions and a moderate phase contrast, the effective stiffness tensor is close to the Neumann stiffness tensor for structures with a scale factor of 3 or higher. The Dirichlet stiffness tensor is close to the effective stiffness tensor for structures with a scale factor of 6 or higher.
- For the stiff matrix microstructure with a high contrast ratio, the effective stiffness tensor is close to the Dirichlet stiffness tensor only for structures with a scale factor of 6 or higher. The Neumann stiffness tensor significantly underestimates the effective stiffness and cannot be used as an estimate of the effective moduli.
- For the compliant matrix microstructure with a high contrast ratio, the Neumann stiffness tensor is close to the effective stiffness tensor for structures with a scale factor of 3 or higher. The Dirichlet stiffness tensor cannot be used as an estimate of the effective moduli for such a composite.
- For the more complex negative Poisson's ratio microstructure with a high contrast ratio, the Dirichlet stiffness tensor for structures with a scale factor of 6 or higher,

gives reasonable estimates of the effective stiffness tensor. The Neumann stiffness tensor significantly underestimates the effective stiffness.

● The Dirichlet and Neumann tensors for the considered examples satisfy the chains of inequalities (45) and (46).

3.4. Bulk and shear moduli behavior

In this section we study the Dirichlet and Neumann bulk and shear moduli for the stiff and compliant matrix composites depicted in Figs 2(a) and (b), respectively. These structures are geometrically square symmetric, which implies square symmetry of the stiffness tensors. We designed them to be isotropic, i.e., with equal shear moduli μ^{I} and μ^{II}. As we observe, however, there is a small difference between the values of these shear moduli which is larger for the cases with a high phase contrast E_1/E_2. We will neglect this small difference and compare the Dirichlet and Neumann shear moduli with the Hashin–Shtrikman shear modulus bounds for isotropic materials.

The numerical values of the bulk and shear moduli are given by the 1×3 matrices in Tables 1–4. We denote Dirichlet and Neumann bulk moduli of the scale factor n structure by $\kappa_{\mathscr{D}}^{(n)}$ and $\kappa_{\mathscr{N}}^{(n)}$, respectively. Figure 4 illustrates the convergence of the numerically computed Dirichlet and Neumann bulk moduli as a function of the scale factor for the maximum bulk modulus microstructure. The dashed line shows the
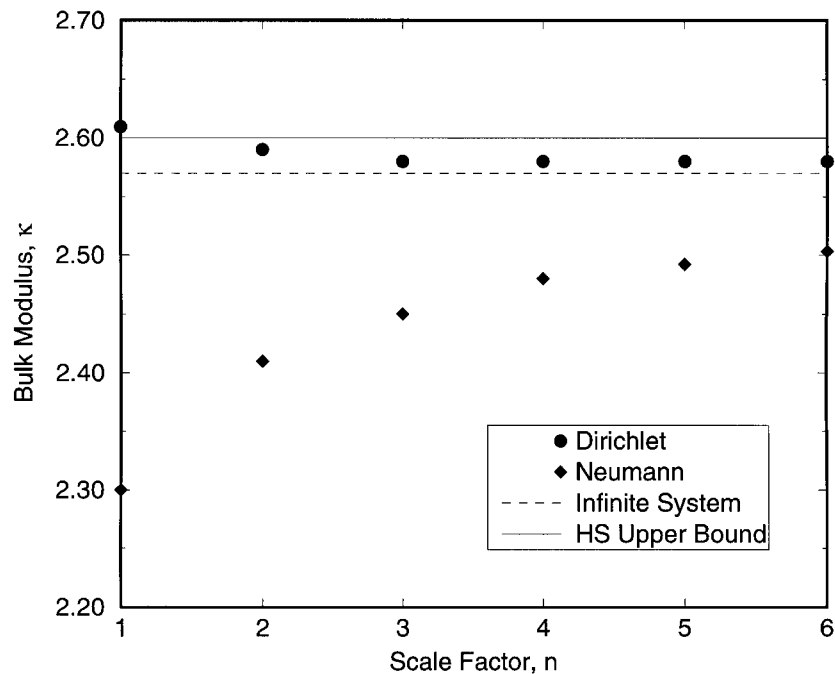

Fig. 4. Convergence of the Dirichlet and Neumann bulk moduli for the stiff composite with increasing scale factor n in which $E_1/E_2 = 10$.

value of the effective bulk modulus (for periodic boundary conditions). The solid line shows the Hashin–Shtrikman bulk modulus upper bound. As one can see, the Dirichlet bulk modulus is always greater than the effective bulk modulus. It converges to the effective bulk modulus and does not violate the Hashin–Shtrikman bound (42), except for the value $\kappa_{\mathscr{D}}^{(1)}$ which exceeds the bound by a small margin. The Neumann bulk modulus converges to the effective bulk modulus from below. Figure 5 illustrates corresponding results for the minimum bulk modulus microstructure. The Neumann bulk modulus does not violate the Hashin–Shtrikman lower bound (41) for any n. Note that the only point that violates the upper bound (40) is the Dirichlet bulk modulus $\kappa_{\mathscr{D}}^{(1)}$. It is interesting to examine whether this is a small numerical error or a real difference.

Let us compare the problems with periodic and Dirichlet boundary conditions for this example. When the unit square (with the square symmetric microstructure) is subject to the periodic or Dirichlet boundary conditions with the average strain $\boldsymbol{a}^{(1)}$, then the cell retains its square shape; However, the Dirichlet restrictions are more severe since they exactly prescribe the displacement for each point on the boundary, whereas the periodic boundary conditions are less demanding. Therefore, the Dirichlet bulk modulus of the structure that has an effective bulk modulus equal to the Hashin–Shtrikman bound (42) may violate this bound. One-scale composites with an effective bulk modulus equal to the Hashin–Shtrikman bound were found by Vigdergauz
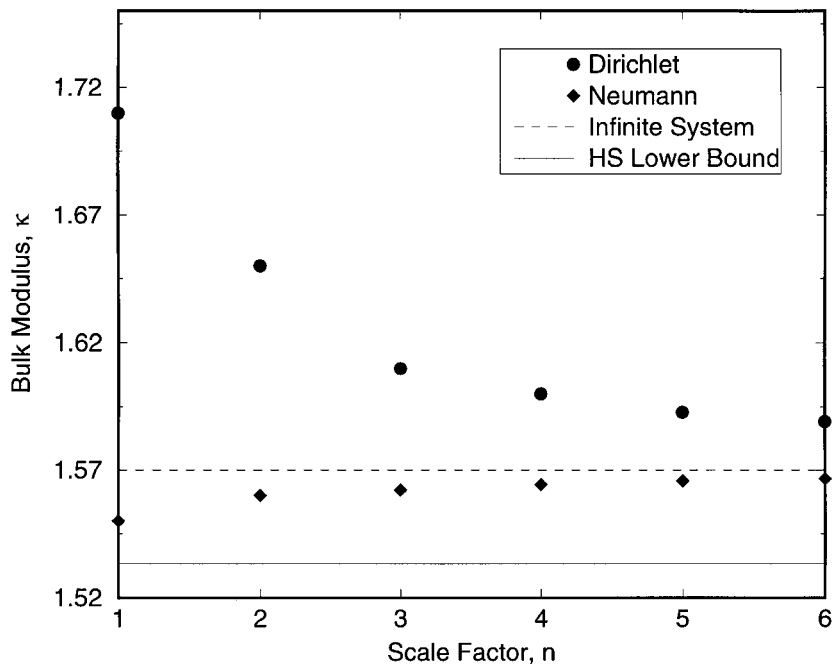

Fig. 5. Convergence of the Dirichlet and Neumann bulk moduli for the compliant composite with increasing scale factor n in which $E_1/E_2 = 10$.

(1989). We may expect that the Dirichlet bulk modulus of those constructions exceeds the bound. Indeed, our calculation of the Dirichlet bulk modulus of the Vigdergauz construction for the phase moduli and volume fractions (48) gives the value $\kappa_{\mathscr{D}}^{(1)} = 2.65$, which is slightly higher than the Hashin–Shtrikman bound $\kappa_{HS}^{U} = 2.60$.

To study the question further, we performed the following numerical experiment on the unit square shown in Fig. 2(a). Instead of applying the Dirichlet boundary conditions to the original elementary cell, we shift this cell by a distance s in the horizontal and vertical directions, with s ranging from 0 to 1/2 (Fig. 6). We confirmed that the effective bulk modulus (for periodic boundary conditions) is not affected by such a shift. However, the Dirichlet bulk modulus $\kappa_{\mathscr{D}}^{(1)}$ is a function of the shift s. Figure 7 illustrates this dependence for the composite with the contrast ratio $E_1/E_2 = 1000$. The dashed line in this figure corresponds to the effective bulk modulus, the solid line shows the Hashin–Shtrikman bound (42) and the dots are the results of our calculations. The plot is symmetric with respect to the axis $s = 0.5$. Indeed, shifts by s_0 and $1 - s_0$ results in the same unit square, rotated by an angle π, which does not change the effective or Dirichlet properties.
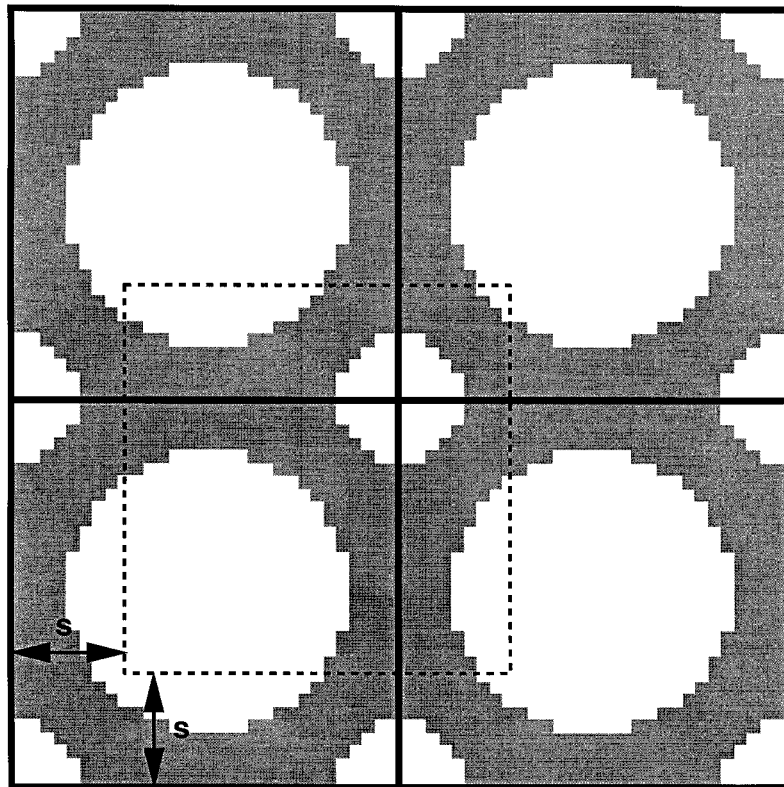

Fig. 6. The window is shifted vertically and horizontally by a value s to study the effect on the Dirichlet and Neumann bulk moduli. The effective (periodic) bulk modulus is unaffected.
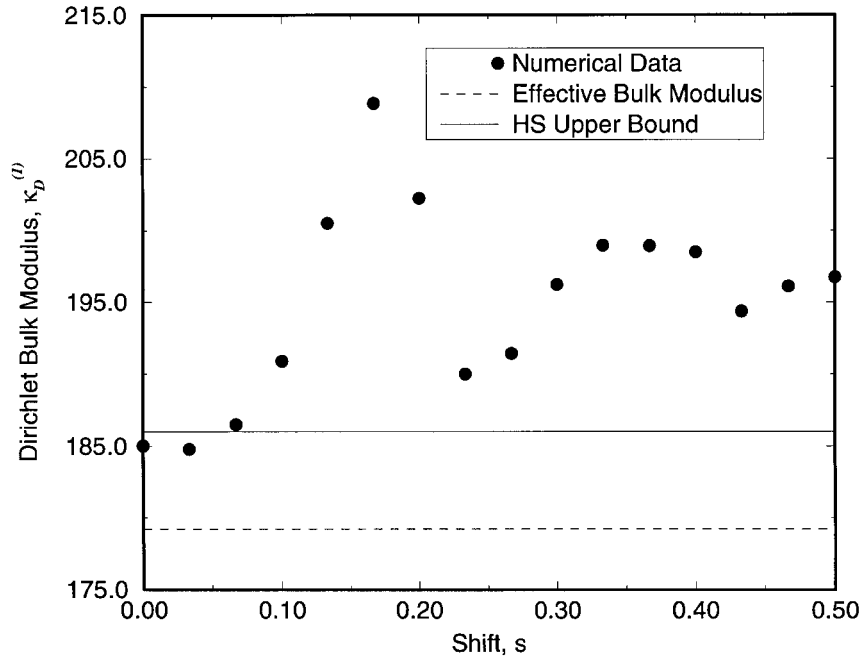
Fig. 7. Dirichlet bulk modulus data for various shifts s of the stiff composite with a contrast ratio of $E_1/E_2 = 1000$.

One can see that the Dirichlet bulk modulus exceeds the bound by as much as 12% for a contrast ratio $E_1/E_2 = 1000$. We observed similar effect for stiff matrix composites with the contrast ratio $E_1/E_2 = 10$. The Dirichlet bulk modulus exceeds the bound by 7% in this case. It is evident now that the upper bound of (47) does not hold. It should be possible to construct bounds that are both independent of the microstructure of the composite and sharper than the arithmetic–harmonic mean bounds. However, such sharper bounds are not available at the moment.

The shear moduli of these structures also do not satisfy the Hashin–Shtrikman shear modulus bounds. In particular, for the structure with scale factor $n = 1$, the Dirichlet shear moduli of the stiff matrix composites (Tables 1 and 3) and the Neumann shear moduli of the compliant matrix composites (Table 2 and 4) violate the corresponding Hashin–Shtrikman shear moduli bounds.

Note however, for the scale factor $n = 2$ structures, this discrepancy is already gone within numerical accuracy. Particularly, the bulk modulus of the scale $n = 2$ Vigdergauz-type microstructure is equal to the Hashin–Shtrikman upper bound within numerical accuracy. Apparent bulk and shear moduli for the shifted $n = 2$ microstructure also fall between the Hashin–Shtrikman bounds. This suggests that these bounds can be used to estimate the apparent moduli of scale $n \geqslant 2$ microstructures.

4. Two-scale composites

We now consider composites with two distinct levels of hierarchy. Such a construction is illustrated in Fig. 8 where a unit square composed of nine cells is shown. The central cell is occupied by a stiff phase 3 and the eight outer cells are composed of two other elastic materials. We will pose two questions: first, can one replace the complex structure of the outer cells with a homogeneous material whose effective property tensor corresponds to the microstructure of those outer cells? Second, how do Dirichlet and Neumann stiffness tensors of such two-scale microstructures differ from the effective property tensors of such structures. As a basis of our analyses, we use the same stiff, compliant matrix and negative Poisson's ratio materials discussed in the previous sections.

The results are summarized in Tables 6–11. The first row of each table shows the microstructure of the unit square. The white material denotes the most compliant phase, dark gray regions represent the stiffer phase and the black core is the most rigid phase. In the case of the stiff and compliant two-scale microstructures, the moduli of phases 1 and 2 are given by (48) and the properties of the rigid phase three are given by
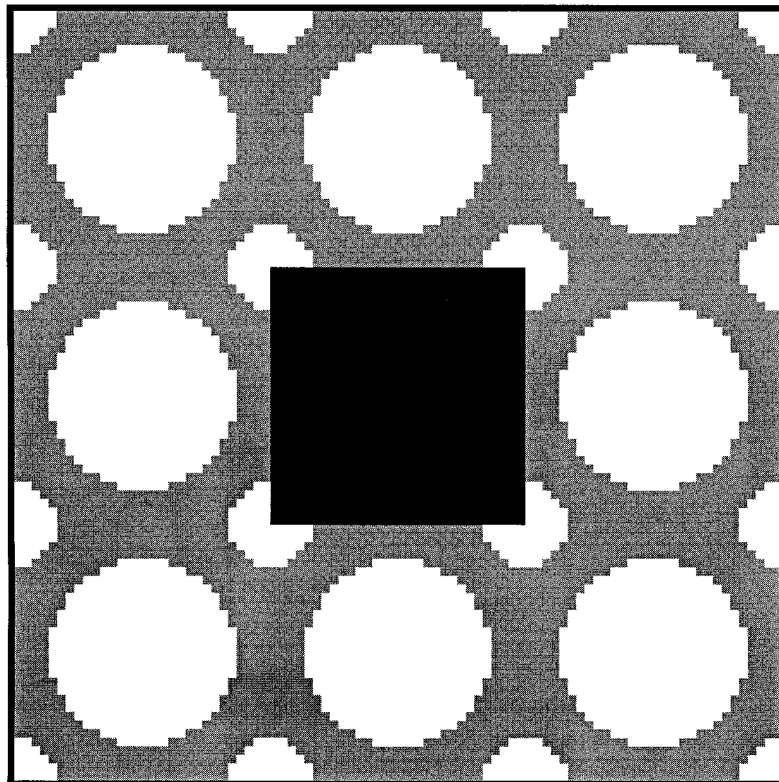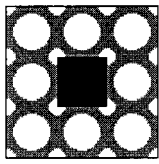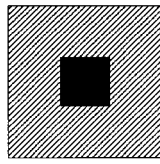

Fig. 8. A composite material with two distinct internal length scales.

Table 6
Results for two-scale maximum bulk modulus microstructure with scale factor $n = 3$ in which $E_1/E_2 = 10$ and $E_3/E_2 = 100$. Stiffness values are given in full tensor form followed by the moduli κ, μ^{I} and μ^{II}, respectively

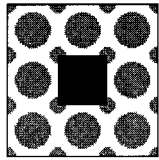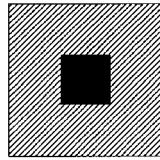| Boundary Conditions		
Dirichlet	$\begin{bmatrix} 4.63 & 1.50 & 0.0 \\ 1.50 & 4.63 & 0.0 \\ 0.0 & 0.0 & 1.64 \end{bmatrix}$ $\begin{bmatrix} 3.07 & 1.57 & 1.64 \end{bmatrix}$	$\begin{bmatrix} 4.51 & 1.54 & 0.0 \\ 1.54 & 4.51 & 0.0 \\ 0.0 & 0.0 & 1.42 \end{bmatrix}$ $\begin{bmatrix} 3.03 & 1.49 & 1.42 \end{bmatrix}$
Periodic	$\begin{bmatrix} 4.49 & 1.60 & 0.0 \\ 1.60 & 4.49 & 0.0 \\ 0.0 & 0.0 & 1.44 \end{bmatrix}$ $\begin{bmatrix} 3.05 & 1.45 & 1.44 \end{bmatrix}$	$\begin{bmatrix} 4.51 & 1.55 & 0.0 \\ 1.55 & 4.51 & 0.0 \\ 0.0 & 0.0 & 1.39 \end{bmatrix}$ $\begin{bmatrix} 3.03 & 1.48 & 1.39 \end{bmatrix}$
Neumann	$\begin{bmatrix} 4.10 & 1.68 & 0.0 \\ 1.68 & 4.10 & 0.0 \\ 0.0 & 0.0 & 1.25 \end{bmatrix}$ $\begin{bmatrix} 2.89 & 1.21 & 1.25 \end{bmatrix}$	$\begin{bmatrix} 4.44 & 1.61 & 0.0 \\ 1.61 & 4.44 & 0.0 \\ 0.0 & 0.0 & 1.38 \end{bmatrix}$ $\begin{bmatrix} 3.03 & 1.42 & 1.38 \end{bmatrix}$

$$E_3 = 100.0, \quad v_3 = 0.3. \tag{58}$$

For the negative Poisson's ratio examples, the moduli of phases 1 and 2 are given by (52) and the properties of the rigid phase three are given by

$$E_3 = 30,000.0, \quad v_3 = 0.3. \tag{59}$$

In the experiment described by the last column of each table, we replace the fine microstructure of the elementary cells by a homogeneous material with corresponding effective properties. This is equivalent to the limit in which all outer cells are refined to make the scale of the elementary cells much smaller than the size of the unit square. The first row of each table gives the Dirichlet stiffness tensors $C_\mathscr{D}^{(1)}$ of the corresponding
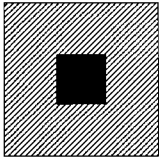
Table 7
Results for two-scale minimum bulk modulus microstructure with scale factor $n = 3$ in which $E_1/E_2 = 10$ and $E_3/E_2 = 100$. Stiffness values are given in full tensor form followed by the moduli κ, μ^{I} and μ^{II}, respectively

Boundary Conditions		
Dirichlet	$\begin{bmatrix} 3.07 & 0.78 & 0.0 \\ 0.78 & 3.07 & 0.0 \\ 0.0 & 0.0 & 1.10 \end{bmatrix}$ $\begin{bmatrix} 1.93 & 1.15 & 1.10 \end{bmatrix}$	$\begin{bmatrix} 2.94 & 0.82 & 0.0 \\ 0.82 & 2.94 & 0.0 \\ 0.0 & 0.0 & 1.06 \end{bmatrix}$ $\begin{bmatrix} 1.88 & 1.06 & 1.06 \end{bmatrix}$
Periodic	$\begin{bmatrix} 2.97 & 0.80 & 0.0 \\ 0.80 & 2.97 & 0.0 \\ 0.0 & 0.0 & 1.04 \end{bmatrix}$ $\begin{bmatrix} 1.89 & 1.09 & 1.04 \end{bmatrix}$	$\begin{bmatrix} 2.94 & 0.82 & 0.0 \\ 0.82 & 2.94 & 0.0 \\ 0.0 & 0.0 & 1.04 \end{bmatrix}$ $\begin{bmatrix} 1.88 & 1.06 & 1.04 \end{bmatrix}$
Neumann	$\begin{bmatrix} 2.85 & 0.89 & 0.0 \\ 0.89 & 2.85 & 0.0 \\ 0.0 & 0.0 & 0.98 \end{bmatrix}$ $\begin{bmatrix} 1.87 & 0.98 & 0.98 \end{bmatrix}$	$\begin{bmatrix} 2.89 & 0.86 & 0.0 \\ 0.86 & 2.89 & 0.0 \\ 0.0 & 0.0 & 1.03 \end{bmatrix}$ $\begin{bmatrix} 1.88 & 1.02 & 1.03 \end{bmatrix}$

structures, the second row corresponds to the effective property tensors $C_* = C_{\mathscr{D}}^{(\infty)} = C_{\mathscr{N}}^{(\infty)}$ and the last row gives the Neumann stiffness tensors $C_{\mathscr{N}}^{(1)}$.

Tables 6–8 summarize the results for the stiff, compliant and negative Poisson's ratio cells. It is interesting to see that the difference between the effective stiffness tensors of the unrefined (with finite separation of scales) and homogenized microstructures is extremely small. The largest difference is for the negative Poisson's ratio matrix which still does not exceed 5%. Therefore, when calculating effective properties, the two-scale microstructure can be replaced by a one scale construction. The effective properties of the material of smallest scale can be used instead of the actual properties in that region. This is true even in the limiting case considered here in which only two periodic cells of the small-scale material lie between elements of the higher-scale structure.

Table 8
Results for two-scale negative Poisson's ratio microstructure with scale factor $n = 3$ in which $E_1/E_2 = 1000$ and $E_3/E_2 = 30\,000$. Stiffness values are given in full tensor form

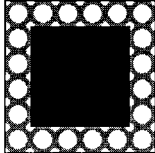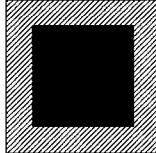| Boundary Conditions		
Dirichlet	$\begin{bmatrix} 96.98 & -29.13 & 0.0 \\ -29.13 & 90.38 & 0.0 \\ 0.0 & 0.0 & 56.24 \end{bmatrix}$	$\begin{bmatrix} 78.09 & -31.87 & 0.0 \\ -31.87 & 74.30 & 0.0 \\ 0.0 & 0.0 & 52.80 \end{bmatrix}$
Periodic	$\begin{bmatrix} 81.93 & -31.17 & 0.0 \\ -31.17 & 75.75 & 0.0 \\ 0.0 & 0.0 & 53.71 \end{bmatrix}$	$\begin{bmatrix} 77.97 & -31.94 & 0.0 \\ -31.94 & 74.17 & 0.0 \\ 0.0 & 0.0 & 52.54 \end{bmatrix}$
Neumann	$\begin{bmatrix} 15.20 & 0.18 & 0.0 \\ 0.18 & 13.39 & 0.0 \\ 0.0 & 0.0 & 4.07 \end{bmatrix}$	$\begin{bmatrix} 77.11 & -32.00 & 0.0 \\ -32.00 & 73.42 & 0.0 \\ 0.0 & 0.0 & 52.37 \end{bmatrix}$

Similar results are valid for the Dirichlet and Neumann stiffness tensors for composites with small contrast ratios as shown in the first and last rows of Tables 6 and 7. The difference for the high contrast negative Poisson's ratio cell is on the order of 20% for the Dirichlet stiffness tensor (Table 8). The Neumann stiffness tensor shows great variation. However, this is consistent with the results of Table 3 which also shows a drastic drop in the magnitude of the stiffness coefficients for Neumann boundary conditions.

Examining the data in each column of the tables (i.e., comparing Dirichlet, Neumann and effective stiffness tensors) we observe that their variance is on the order of the difference for the $n = 3$ composites in the previous section. This is reasonable since most of the difference is caused by boundary effects. The stiffness of the central square (which is the stiff phase 3 in this section and the same elementary cell in the examples of the previous section) affects the overall properties but not the relative difference of the stiffness tensors.

Table 9–11 show the results of similar calculations where the scale of the stiff core has been increased to two thirds the size of the unit square. It is interesting to observe that this actually decreases the difference between the unrefined and homogenized

Table 9
Results for two-scale maximum bulk modulus microstructure with scale factor $n = 6$ in which $E_1/E_2 = 10$ and $E_3/E_2 = 100$. Stiffness values are given in full tensor form followed by the moduli κ, μ^{I} and μ^{II}, respectively

Boundary Conditions		
Dirichlet	$\begin{bmatrix} 9.22 & 2.02 & 0.0 \\ 2.02 & 9.22 & 0.0 \\ 0.0 & 0.0 & 3.12 \end{bmatrix}$ $\begin{bmatrix} 5.62 & 3.60 & 3.12 \end{bmatrix}$	$\begin{bmatrix} 8.93 & 2.03 & 0.0 \\ 2.03 & 8.93 & 0.0 \\ 0.0 & 0.0 & 2.79 \end{bmatrix}$ $\begin{bmatrix} 5.48 & 3.45 & 2.79 \end{bmatrix}$
Periodic	$\begin{bmatrix} 8.94 & 2.01 & 0.0 \\ 2.01 & 8.94 & 0.0 \\ 0.0 & 0.0 & 2.32 \end{bmatrix}$ $\begin{bmatrix} 5.48 & 3.47 & 2.32 \end{bmatrix}$	$\begin{bmatrix} 8.85 & 1.96 & 0.0 \\ 1.96 & 8.85 & 0.0 \\ 0.0 & 0.0 & 2.22 \end{bmatrix}$ $\begin{bmatrix} 5.41 & 3.45 & 2.22 \end{bmatrix}$
Neumann	$\begin{bmatrix} 7.60 & 2.76 & 0.0 \\ 2.76 & 7.60 & 0.0 \\ 0.0 & 0.0 & 2.01 \end{bmatrix}$ $\begin{bmatrix} 5.18 & 2.42 & 2.01 \end{bmatrix}$	$\begin{bmatrix} 8.09 & 2.70 & 0.0 \\ 2.70 & 8.09 & 0.0 \\ 0.0 & 0.0 & 2.14 \end{bmatrix}$ $\begin{bmatrix} 5.40 & 2.70 & 2.14 \end{bmatrix}$

unit squares. Since the small scale microstructure has now become even smaller compared to the unit square, there is less error associated with replacing the structure by its corresponding homogeneous material.

Summarizing the results of this section we formulate the following statements:

- Replacement of the smallest-scale microstructure by the equivalent (in the sense of the effective properties) homogeneous material does not cause large error in calculation of the effective stiffness tensors of these structures for any phase contrast ratio.
- Such a replacement does not cause large error in the Dirichlet and Neumann stiffness tensors for moderate ($E_1/E_2 = 10$ in our examples) contrast ratios, but may lead to large error for higher contrast ratios on the order of $E_1/E_2 = 1000$.

Table 10
Results for two-scale minimum bulk modulus microstructure with scale factor $n = 6$ in which $E_1/E_2 = 10$ and $E_3/E_2 = 100$. Stiffness values are given in full tensor form followed by the moduli κ, μ^I and μ^{II}, respectively
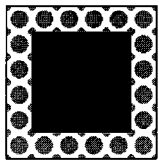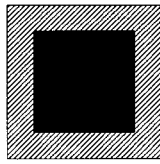
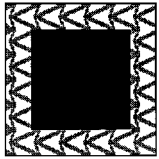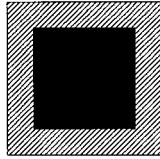| Boundary Conditions		
Dirichlet	$\begin{bmatrix} 6.10 & 1.05 & 0.0 \\ 1.05 & 6.10 & 0.0 \\ 0.0 & 0.0 & 2.10 \end{bmatrix}$ $\begin{bmatrix} 3.58 & 2.53 & 2.10 \end{bmatrix}$	$\begin{bmatrix} 5.99 & 1.10 & 0.0 \\ 1.10 & 5.99 & 0.0 \\ 0.0 & 0.0 & 2.05 \end{bmatrix}$ $\begin{bmatrix} 3.55 & 2.45 & 2.05 \end{bmatrix}$
Periodic	$\begin{bmatrix} 5.97 & 1.00 & 0.0 \\ 1.00 & 5.97 & 0.0 \\ 0.0 & 0.0 & 1.68 \end{bmatrix}$ $\begin{bmatrix} 3.49 & 2.49 & 1.68 \end{bmatrix}$	$\begin{bmatrix} 5.92 & 1.04 & 0.0 \\ 1.04 & 5.92 & 0.0 \\ 0.0 & 0.0 & 1.67 \end{bmatrix}$ $\begin{bmatrix} 3.48 & 2.44 & 1.67 \end{bmatrix}$
Neumann	$\begin{bmatrix} 5.38 & 1.52 & 0.0 \\ 1.52 & 5.38 & 0.0 \\ 0.0 & 0.0 & 1.56 \end{bmatrix}$ $\begin{bmatrix} 3.45 & 1.93 & 1.56 \end{bmatrix}$	$\begin{bmatrix} 5.44 & 1.50 & 0.0 \\ 1.50 & 5.44 & 0.0 \\ 0.0 & 0.0 & 1.61 \end{bmatrix}$ $\begin{bmatrix} 3.47 & 1.97 & 1.61 \end{bmatrix}$

- The Dirichlet and Neumann stiffness tensors of the two-scale structures are as close (or closer) to the effective stiffness tensors of these structures as the corresponding one-scale structures with appropriate scale factor.
- For stiff matrix microstructures, the Dirichlet stiffness tensor is closer to the effective stiffness tensor.
- For compliant matrix microstructures, the Neumann stiffness tensor is closer to the effective stiffness.

5. Conclusions and discussion

We have investigated numerically the stiffness of one- and two-scale composites for three types of boundary conditions (Dirichlet, Neumann and periodic), three types

Table 11
Results for two-scale negative Poisson's ratio microstructure with scale factor $n = 6$ in which $E_1/E_2 = 1000$ and $E_3/E_2 = 30\,000$. Stiffness values are given in full tensor form

Boundary Conditions		
Dirichlet	$\begin{bmatrix} 188.80 & -27.80 & 0.0 \\ -27.82 & 175.47 & 0.0 \\ 0.0 & 0.0 & 98.26 \end{bmatrix}$	$\begin{bmatrix} 172.72 & -29.84 & 0.0 \\ -29.85 & 165.02 & 0.0 \\ 0.0 & 0.0 & 93.41 \end{bmatrix}$
Periodic	$\begin{bmatrix} 171.81 & -30.21 & 0.0 \\ -30.21 & 159.18 & 0.0 \\ 0.0 & 0.0 & 87.90 \end{bmatrix}$	$\begin{bmatrix} 165.38 & -31.15 & 0.0 \\ -31.15 & 157.41 & 0.0 \\ 0.0 & 0.0 & 85.79 \end{bmatrix}$
Neumann	$\begin{bmatrix} 32.32 & 0.31 & 0.0 \\ 0.31 & 28.79 & 0.0 \\ 0.0 & 0.0 & 7.80 \end{bmatrix}$	$\begin{bmatrix} 158.42 & -36.61 & 0.0 \\ -36.61 & 150.94 & 0.0 \\ 0.0 & 0.0 & 83.33 \end{bmatrix}$

of elementary cells (see Fig. 2) and two phase contrast ratios ($E_1/E_2 = 10$ and $E_1/E_2 = 1000$). For the one-scale composite, we observed that the Dirichlet stiffness tensor always overestimates the effective stiffness tensor while the Neumann stiffness tensor always provides an underestimate, all of which is consistent with known rigorous bounds (Huet, 1990; Hazanov and Huet, 1994). Initially, it appeared that the Dirichlet, Neumann and effective bulk moduli all obey the Hashin–Shtrikman bounds. However, a more detailed investigation provided a counterexample when the Dirichlet bulk modulus of a scale 1 structure significantly exceeded the Hashin–Shtrikman bulk modulus upper bound. We also found that the Dirichlet and Neumann shear moduli may violate the corresponding Hashin–Shtrikman shear modulus bounds. However, the Hashin–Shtrikman bounds are a good approximation for bounds on the moduli of composites with a scale factor $n = 2$ or higher.

The difference between the effective stiffness tensor and the tensors computed using Dirichlet and Neumann boundary conditions depends strongly on the phase contrast ratio. We have found that the Dirichlet stiffness tensor is more accurate than the Neumann stiffness tensor (i.e. closer to the effective stiffness tensor) for stiff matrix composites. Conversely, the Neumann stiffness tensor is more accurate for compliant

matrix composites. This is explained by the behavior of the fields near boundary of the unit square. More complex structures should be analyzed individually following the guidelines developed in analyses of stiff matrix and compliant matrix composites.

Our results show a strong influence of the boundary conditions on the apparent stiffness of the composite sample. We observe that even at scale 6, there is a significant difference between the Dirichlet and the Neumann stiffness tensors. Our results show that inhomogeneous materials require rigorous accounting for the decay of the boundary effect, especially for the composites with high phase contrast ratio. The size of the RVE for high-contrast composites may be much larger than those for composites with similar phase stiffnesses.

For the hierarchical composite with two distinct length scales, we conclude that replacing the smallest-scale microstructure by an equivalent homogeneous material causes very little error in the three types of stiffness tensors, even when the ratio of the two length scales is as small as three. This error becomes even less significant as the difference in scale becomes larger. The variance between the effective stiffness tensor and the corresponding Dirichlet and Neumann tensors is not greater than in the one-scale case. Thus, homogenization can offer great convenience in reducing the complexity of computing effective properties of two-scale composites and hierarchical composites in general.

Acknowledgements

References

Bensoussan, A., Lions, J.L., Papanicolaou, G., 1978. Asymptotic Analysis for Periodic Structures. North Holland, Amsterdam.

Bourgat, J., 1977. Numerical experiments of the homogenization method for operators with periodic coefficients. Lecture Notes in Mathematics 704, 330–356.

Christensen, R.M., 1979. Mechanics of Composite Materials. John Wiley and Sons.

Drugan, W.J., Willis, J.R., 1996. A micromechanics-based nonlocal constitutive equation and estimates of representative volume element size for elastic composites. Journal of the Mechanics and Physics of Solids 44, 497–524.

Guedes, J., Kikuchi, N., 1991. Preprocessing and postprocessing for materials based on the homogenization method with adaptive finite element methods. Computer Methods in Applied Mechanical Engineering 83, 143–198.

Hashin, Z., 1965. On elastic behaviour of fiber reinforced materials of arbitrary transverse phase geometry. Journal of the Mechanics and Physics of Solids 13, 119–134.

Hashin, Z., 1983. Analysis of composite materials. ASME Journal of Applied Mechanics 50, 481–505.

Hashin, Z., Shtrikman, S., 1963. A variational approach to the theory of the elastic behavior of multiphase materials. Journal of the Mechanics and Physics of Solids 11, 127–140.

Hazanov, S., Amieur, M., 1995. On overall properties of elastic heterogeneous bodies smaller than the representative volume. International Journal of Engineering Science 33, 1289–1301.

Hazanov, S., Huet, C., 1994. Order relationships for boundary conditions effect in heterogeneous bodies smaller than representative volume. Journal of the Mechanics and Physics of Solids 42, 1995–2011.

Hill, R., 1952. The elastic behavior of a crystalline aggregate. Proc. Phys. Soc. London A 65, 349–354.

Huet, C., 1990. Application of variational concepts to size effects in elastic heterogeneous bodies. Journal of the Mechanics and Physics of Solids 38, 813–841.

Ostoja-Starzewski, M., 1993. Micromechanics as a basis of random continuum approximations. Probabilistic Engineering Mechanics 8, 107–114.

Ostoja-Starzewski, M., 1996. Bounding of effective thermal conductivities of multiscale materials by essential and natural boundary conditions. Physical Review B 54, 278–285.

Ostoja–Starzewski, M., 1998. Random field models of heterogeneous materials. Int. J. Solids Structures 35, 2429–2455.

Prevost, J.H., 1997. DYNAFLOW Version v98 finite element solver.

Sanchez-Palencia, E., 1980. Nonhomogeneous media and vibration theory. In: Lecture Notes in Physics. Springer-Verlag, Berlin.

Sigmund, O., Torquato, S., Aksay, I.A., 1998. On the design of 1–3 piezocomposites using topology optimization. Journal of Materials Science Research, in press.

Vigdergauz, S., 1989. Regular structures with extremal elastic properties. Mechanics of Solids 24, 57–63.

Willis, J.R., 1977. Bounds and self-consistent estimates for the overall properties of anisotropic composites. Journal of the Mechanics and Physics of Solids 25, 185–202.